To the Graduate Council:

I am submitting herewith a thesis written by Jaein Suh entitled "Processing and Properties of Melt-Spun and Drawn 2-Methyl-1,3-Propanediol Substituted Poly(ethylene terephthalate." I have examined the final copy of this thesis for form and content and recommend that it be accepted in partial fulfillment of the major requirements for the degree of Master of Science, with a major in Polymer Engineering.

Joseph E. Spruiell, Major Professor

We have read this thesis and recommend its acceptance:

John F. Fellers

Roberto Benson

Accepted for the Council:

Interim Vice Provost

and Dean of the Graduate School

Processing and Properties of Melt-Spun and Drawn 2-Methyl-1,3-Propanediol Substituted Poly(ethylene terephthalate)

A Thesis Presented for the Master of Science Degree

The University of Tennessee, Knoxville

Jaein Suh

August 2001

ACKNOWLEDGEMENT

I would like to express sincere thanks to Dr. Joseph E. Spruiell for his thorough advice and guidance through this investigation. Thanks goes to the Lyondell Chemical Company for funding and supplying materials used in this study.

I am indebted to the members of Dr. Spruiell's group: Melissa Williams, Gary Holt, Chris Lewis and Xiaoyun Ling. Special thanks go to Jeongihm Pak and Dr. Marek Pyda in the Chemistry Department for their help in DSC measurements. I also would like to thank Doug Fielden and Greg Jones for their technical support.

Finally, I would like to express my deepest gratitude to my wife, Tae-Eun Chang, my parents and family for their love and support.

ABSTRACT

The preparation of fibers from copolymers of PET in which up to 25 mol% 2-methyl-1,3-propanediol (referred to as MPDiol) was substituted for ethylene glycol were studied. The purpose of this study was to determine if the copolymers provided any specific advantages over PET homopolymer in either processing or properties. Filaments were melt spun from resins containing 0, 4, 7, 10 and 25 mol% MPDiol over a range of spinning conditions, including spinning at speeds up to about 5500 m/min and mass throughputs between about 1.15 and 8.25 g/min/hole. Some filaments that were melt spun at low speeds were subjected to hot drawing. Characterization of the filaments was carried out by measurement of filament diameter, birefringence, DSC crystallinity, wide angle X-ray diffraction patterns, boiling water shrinkage, tenacity and elongation to break. The results showed that the 25% MPDiol substituted resin did not crystallize in the spinline at any spinning speed investigated. The other resins did crystallize in the spinline at high spinning speeds, but, compared to the PET homopolymer, increasing substitution of MPDiol reduced the rate at which crystallinity of the melt spun filaments increased with spinning speed. Increasing MPDiol also reduced the ultimate crystallinity that could be achieved by high speed spinning (about 33% for PET homopolymer and 22% for the 10 mol% MPDiol substituted resin). The rate of development of molecular orientation, as measured by birefringence, also decreased somewhat with increasing MPDiol content. Shrinkage in boiling water decreased at high spinning speeds as the amount of crystallinity developed increased; however, the shrinkage decreased more slowly with increase in spinning speed as MPDiol content increased due to the slower development of crystallinity. Tenacity also decreased slightly at any given spinning speed as MPDiol

content increased, but there was no significant effect on the elongation-to-break. A major advantage of adding MPDiol is that increasing substitution of MPDiol up to 7 mol% increased the maximum take-up velocity that could be achieved at a given mass throughput. This could potentially increase the productivity of melt spun yarns via the use of higher spinning speeds. Drawn samples containing 10 mol% MPDiol were readily processed into highly oriented fibers having slightly less birefringence, crystallinity and tenacity than similarly processed PET homopolymer.

TABLE OF CONTENTS

CHAPTER			PAGE
1	**Introduction**		**1**
2	**Background and Literature Review**		**3**
	2.1	General Background	3
	2.2	Basic Structure of Poly(ethylene terephthalate)	5
		2.2.1 Synthesis and Chemical Structure	5
		2.2.2 Crystal Structure	7
	2.3	Crystallization Kinetics	9
		2.3.1 Isothermal Crystallization	10
		2.3.2 Nonisothermal Crystallization	11
	2.4	Melt Spinning Fundamentals	11
		2.4.1 Crystallization Kinetics in Melt Spinning	11
		2.4.2 Modeling of the Melt Spinning Process	13
		2.4.3 Structure Development in Melt Spinning of PET	19
	2.5	Poly(ethylene terephthalate) Copolymers	25
		2.5.1 General Background	25
		2.5.2 Crystalline Part of Copolymers	26
		2.5.3 Amorphous Part of Copolymers	27
		2.5.4 Properties of PET Copolymers	28
3	**Materials, Processing and Characterization**		**31**
	3.1	Materials	31
	3.2	Processing	31

	3.2.1	Melt Spinning Procedure	31
	3.2.2	Post-Spinning Procedure – Drawing	33
3.3		Filament Characterization	35
	3.3.1	Optical Birefringence	35
	3.3.2	Differential Scanning Calorimetry (DSC)	36
	3.3.3	Shrinkage in Boiling Water	37
	3.3.4	Tensile Analysis	37
	3.3.5	Wide Angle X-ray Diffraction (WAXD)	38
4	**Result and Discussion**		**40**
4.1		Melt Spun Filaments Prepared with Air Drag Device	40
	4.1.1	DSC Crystallinity	40
	4.1.2	Optical Birefringence	42
4.2		Filaments Wound on a Godet	46
	4.2.1	DSC Crystallinity	46
	4.2.2	Optical Birefringence	48
	4.2.3	WAXD Patterns	48
	4.2.4	Shrinkage	52
	4.2.5	Tensile Properties	54
4.3		Filament Spinnability	54
4.4		Drawing of Spun Filaments	57
4.5		Further Discussion of Results	63
5	**Conclusions and Recommendations**		**66**
5.1		Summary and Conclusions	66

5.2 Recommendations for Further Study 67

List of References **69**

Vita **75**

LIST OF TABLES

TABLE		PAGE
3.1	Temperatures used for the drawing process	34
4.1	As-spun filaments wound on bobbins for drawing	57

LIST OF FIGURES

FIGURE		PAGE
2.1	Two-stage ester interchange process of the formation of poly(ethylene terephthalate)	6
2.2	Schematic of crystal structure of poly(ethylene terephthalte)	8
2.3	Chemical structures of 2,3-dialkyl-1,4-butanediols	29
2.4	Chemical structures and codes of 2,2-dialkyl-1,3-propanediols	29
3.1	Schematic of the system used for post-spinning drawing	33
3.2	Schematic of wide angle x-ray diffraction (WAXD) unit	39
4.1	Crystallinity of air drag spun filaments prepared with a nominal mass throughput of around 2.1 g/min/hole	41
4.2	Comparison of crystallinity of PET filaments spun at two different mass throughputs	41
4.3	Birefringence of air drag spun filaments prepared with a nominal mass throughput of 2.1 g/min/hole (8.6 g/min/4holes)	43
4.4	Birefringence of air drag spun filaments prepared with a nominal mass throughput of 1.25 g/min/hole (5 g/min/4holes)	45
4.5	Crystallinity of filaments wound on a 6.25-inch diameter godet with a mass throughput of 2.15 g/min/hole	47
4.6	Comparison of crystallinity between two different mass throughputs of PET homopolymer and 10 mol% MPDiol PET copolymer	47
4.7	Birefringence of filaments spun with a godet draw-down and a nominal mass throughput of 2.15 g/min/hole	49

FIGURE PAGE

4.8 Birefringence of filaments spun with a godet draw-down and a nominal mass throughput of 6.5 g/min/hole 49

4.9 X-ray patterns of selected filaments at the indicated take-up velocities and mass throughputs 51

4.10 Boiling water shrinkage of filaments spun at 2.15 g/min/hole as a function of take-up velocity and MPDiol content 53

4.11 Boiling water shrinkage of filaments spun at 6.5 g/min/hole as a function of take-up velocity and MPDiol content 53

4.12 Tenacity as a function of take-up velocity and MPDiol content for as-spun filaments prepared with a mass throughput of 2.15 g/min/hole 55

4.13 Tenacity as a function of take-up velocity and MPDiol content for as-spun filaments prepared with a mass throughput of 6.5 g/min/hole 55

4.14 Strain at break as a function of take-up velocity and MPDiol content for as-spun filaments prepared with at mass throughput of 2.15 g/min/hole. 56

4.15 Strain at break as a function of take-up velocity and MPDiol content for as-spun filaments prepared with at mass throughput of 6.5 g/min/hole 56

4.16 Maximum take-up velocity as a function of MPDiol content and mass Throughput 58

4.17 Maximum draw ratios as a function of MPDiol composition and different combinations of hot plate and first godet temperatures 60

4.18 Birefringence of fibers drawn with different combinations of hot plate and first godet temperatures 60

FIGURE **PAGE**

4.19 Tenacity of drawn filaments of 10% MPDiol compared to filaments of PET homopolymer 62

4.20 Strain at break for drawn filaments of 10% MPDiol compared to PET homopolymer 62

4.21 X-ray patterns of selected drawn fibers 64

CHAPTER 1

INTRODUCTION

Poly(ethylene terephthalate) (PET) is one of the most widely used polymers for the formation of man-made fibers for the textile market and also has wide applications in industrial usages.

Since PET fiber first became available in the U.S in 1953, the worldwide and U.S. production of PET expanded enormously, especially, in 1960 and 1970s. Although the rate of increase has fallen somewhat, PET continues to be the fastest-growing fiber world wide, with the great versatility of high strength, high modulus, low shrinkage, heat-set ability, light fastness, chemical resistance and so on [1, 2].

With the aim of improving the properties of PET, the modification of PET also has been an attractive subject to many investigators. Numerous studies have been done with the aim of keeping the bright side of PET properties and improving the less desirable properties of PET such as poor dyeability, pilling, low moisture regain and generation of static charges [3~7].

The purpose of the present study is to determine whether copolymers of PET in which 2-methyl-1,3-propanediol (- $HOCH_2C(CH_3)_2CH_2OH$ -, henceforth referred to as MPDiol) is partially substituted for ethylene glycol, have any specific advantages over PET homopolymer. In this study, processing of PET copolymers also involves melt spinning PET copolymers with several different MPDiol compositions, different mass throughputs and take-up velocities. Some of the PET copolymers also were processed after melt spinning by the post spinning procedure– drawing. All filaments were characterized. In particular, this study is concerned with the measurement and

understanding of orientation, crystallinity, thermal and mechanical properties of MPDiol substituted PET copolymers. In all cases, the aim is to determine optimum conditions for producing MPDiol substituted PET copolymers. The overall goal was to establish whether MPDiol substituted resins may surpass PET homopolymer in certain properties or in productivity without sacrificing physical properties or the ability to achieve fine deniers.

CHAPTER 2

BACKGROUND AND LITERATURE REVIEW

2.1 General Background

A polyester fiber, usually represented by poly(ethylene terephthalte) is defined by G. W. Davis and E. S. Hill as "a manufactured fiber in which the fiber forming substance is any long chain synthetic polymer composed of at least 85% by weight of an ester of a dihydric alcohol (HOROH) and terephthalic acid (p-$HOOCC_6H_4COOH$)" [8].

Poly(ethylene terephthalate), commonly called PET, is one of the most widely used polyester fibers and the first fundamental research on PET fibers was done by Carothers and Hill, as a part of the classical work of Carothers in the early 1930s. They had produced fiber-forming aliphatic polyesters, but these products had low melting points and were unsuitable for commercial use [9]. In 1941, J. R. Whinfield and J. T. Dickson recognized the useful fiber-forming properties of PET in the laboratories of Calico Printers Assoc., Ltd. in the UK. Du Pont acquired the U.S. patent rights to manufacture PET fibers in 1948, and the Imperial Chemical Industries, Ltd. of the UK purchased patent rights for the rest of the world [10, 11].

Only a few studies were done during the period 1930~1950 on the synthesis of linear copolyesters. Foremost among these are the x-ray study by C. S. Fuller [12] in 1938 on aliphatic copolyesters such as polyethylene sebacate/adipate, and the confirmation studies on the theory of melting point depression of aliphatic copolyesters by P. J. Flory [13] during the 1940's.

The linear aromatic copolyesters were at first developed in the midst of the 1940's by Wingfoot Corporation in the United States, using an acid chloride. Several patents

appeared pertaining to the production of polyethylene terephthalate/isophthalate, mainly for film-forming polymer by an acid chloride method. In early 1950's, a patent [14] covering the improvement of PET fiber for better dyeability and better water absorbability by copolymerizing alkylene oxides was submitted by Imperial Chemical Industries. At the same time, many analogous patents were submitted, most of which contained various kinds of acids or alcohols as a third component in the polymer, in addition to terephthalic acid and ethylene glycol as main components.

Even though PET fibers have high melting point, crease resistance, and high tensile strength, the limitations encountered in the development of PET fibers for clothes include difficulty of dyeing, the problem of pilling, and the hard touch of the clothing. Many attempts were made to copolymerize a third component in addition to terephthalic acid and ethylene glycol as the main components, the purpose being to eliminate the those limitations mentioned above, especially to improve the poor dyeability and those studies made it possible to manufacture Dacron 64 by Du Pont and Fiber K by Chemstrand [1].

In order to improve a certain portion of the physical properties and keep other properties of the original PET fibers, the amount of the third component is carefully maintained small. The addition of an appreciable amount of the third component not only improved dyeability but also gave a new fiber, distinguished from the original PET fiber in quality.

The modification of PET fibers has been attractive to numerous investigators since PET is the one of the fastest-growing fibers in the world, even though the rate of increase has fallen off somewhat, and in that great versatility of PET fibers such as high

strength, high modulus, heat-set ability, light fastness, and chemical resistance can be still maintained with the modification.

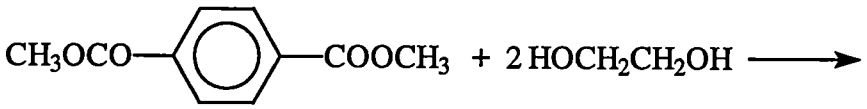
2.2 Basic Structure of Poly(ethylene terephthalate)

2.2.1 Synthesis and Chemical Structure

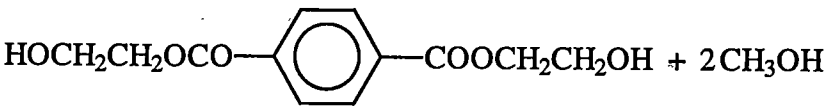
The most straightforward method, which can be formulated for the production of polyester, is to condense the appropriate diol with the chosen dicarboxylic acid. High molecular weight polyester should be expected from the completion of the reaction between equal molecular amounts of the diol and the acid, with the elimination of water. Only low molecular weight material, however, is produced directly from this reaction since the required stoichiometric amount cannot be kept with the necessary accuracy. The ester interchange reaction, therefore, has been used dominantly in the manufacturing processes [1].

The two-stage ester interchange process from dimethyl terephthalate and ethylene glycol produces poly(ethylene terephthalate) as illustrated in **Figure 2.1**. An ester interchange reaction is made at the first stage to produce bis(2-hydroxyethyl)terephthalate along with small amounts of larger-sized oligomers. During this first reaction, the reactants are heated from 150 °C up to 210 °C and the methanol is continuously distilled off. In the second stage, the monomer produced in the first stage is polymerized with the temperature raised to 270-280 °C and the removal of ethylene glycol being facilitated by using a partial vacuum of 0.5-1 torr. The first stage of the polymerization is a solution polymerization, while the second stage is a melt polymerization since the reaction temperature is above the crystalline melting temperature of the polymer [15].

(a) First-stage

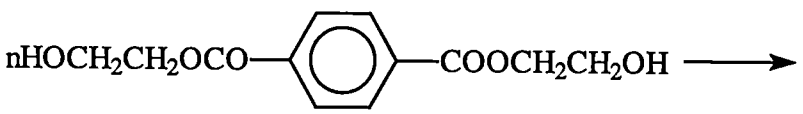


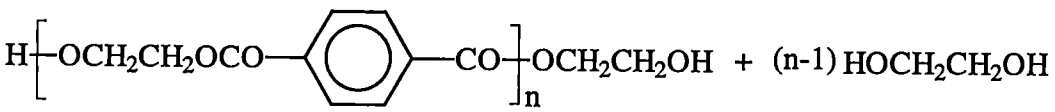
dimethyl terephthalate *ethylene glycol*



bis(2-hydroxyethyl) terephthalate

(b) Second-stage





poly(ethylene terephthalate) (PET)

Figure 2.1 Two-stage ester interchange process of the formation of poly(ethylene terephthalate).

2.2.2 Crystal Structure

The crystal structure of PET has been determined from x-ray diffraction techniques by Daubeny, Bunn, and Brown [16]. The crystal lattice for PET is triclinic, and the lattice parameters are a = 4.56 Å, b = 5.94 Å, c = 10.75 Å, $\alpha = 98.5°$, $\beta = 118°$, $\gamma = 112°$. The molecular chains are nearly planar in configuration, with the aromatic rings almost parallel to the (100) plane as shown in **Figure 2.2** and the ethyl groups depart from the plane by a 20° rotation about the O-CH_2 bond axis. The aromatic, carboxyl, and aliphatic molecular groups, contained in one repeating unit, are almost fully extended along the c-axis and exist in a side-by-side arrangement [16].

The preference for gauche states of the CH_2-CH_2 bonds of PET is presumably responsible for the relatively low crystallization rate of this polymer from the melt. The crystallization behavior of PET makes it feasible to not only obtain this polymer in the amorphous state by quenching from the melt but also to prepare PET with the desired degree of crystallinity by controlling the crystallization rate.

The density of purely crystalline PET determined from the unit cell calculation above is 1.455 g/cm^3 [16] and the density of amorphous PET is 1.33 g/cm^3. The density of amorphous PET increases to 1.38-1.40 g/cm^3, with the increase of the orientation and crystallinity [17].

Distances between atoms in neighboring molecular chains are all normal van der Waals contact distances, and there is no structural evidence for any remarkable intermolecular forces. The reason of the high melting temperature of PET compared with aliphatic polyesters, therefore, can be explained by the cohesion of PET chains induced

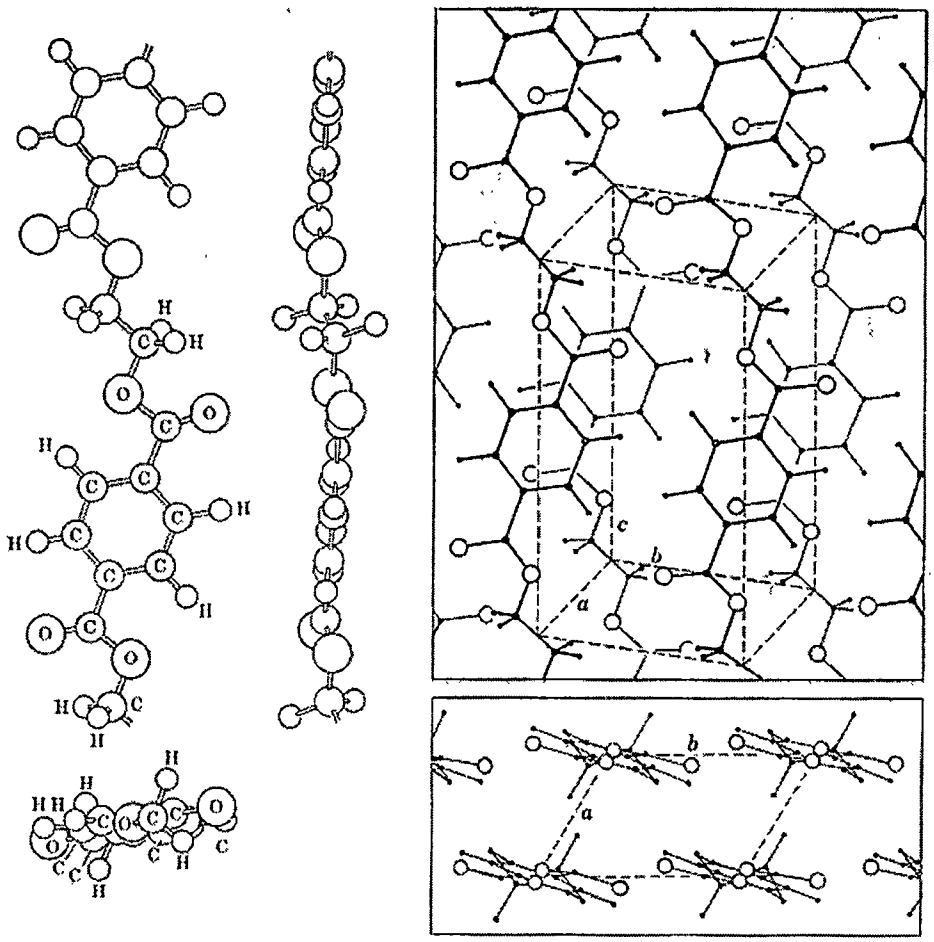


Figure 2.2 Schematic of crystal structure of poly(ethylene terephthalte).

by the van der Waals forces resulting from dipole, induction, and dispersion effects, and the bridging hydrogen bonds [2].

2.3 Crystallization Kinetics

Crystalline PET fibers have distinct characteristics from other crystalline solids in that the former are usually only semicrystalline as are most other polymers. The degree of crystallinty from the semicrytalline properties of polymeric materials, has enormous influences on their physical and mechanical properties, with the crystallite size and its arrangements. It is, therefore, necessary to understand the crystallization behavior of the polymers in order to explain these properties and optimize the polymer processing.

Crystallization is the process whereby an ordered structure is produced from a disordered phase such as a melt or dilute solution and generally consisting of two steps; primary nucleation and crystal growth. Crystal growth follows the primary nucleation, where crystalline or ordered cells form and molecules initiate crystallization. These events are functions of conditions such as time, temperature, pressure, mechanical forces and pretreatment [18].

There are two types of primary nucleation, homogeneous and heterogeneous. In the latter, a nucleus form at the interface with a second phase, which may be impurities or nucleating agents, while homogeneous nucleation is the random formation of nuclei throughout the melt without the presence of a second phase. The spontaneous aggregation of polymer chains reversible by thermal motion is observed in homogeneous nucleation and the heterogeneous nucleation is the predominant form of nucleation of processed polymers and thermoplastic composites.

In a polymer processing operation, it is necessary to understand a nonisothermal crystallization and a crystallization rate as a function of temperature and molecular orientation in order to elucidate crystallization mathematically, since the crystallization almost always occurs under nonisothermal conditions and frequently in the presence of molecular orientation. Numerous investigations have been made on the isothermal crystallization because this is a simple way to examine the effect of crystallization temperature without the complications of changing temperature, pressure or molecular orientation.

2.3.1 Isothermal Crystallization

The degree of phase transformation from amorphous to crystalline phase is related to time t by the general Avrami equation [19]

$$X(t) = 1 - \exp(-kt^n) \quad \text{----------(1)}$$

where k is the overall crystallization rate constant containing nucleation and growth rates, and n is a constant called as the Avrami index, characteristic of the nucleation mode and the crystal growth geometry. It is possible to obtain the values of k and n by fitting isothermal kinetics data and the Avrami index may show values ranging from below 1 and to far above 6 [20]. A plot of $\ln[-\ln(1-X(t))]$ versus ln(t), often referred to as an Avrami plot, should be theoretically linear with n being the slope and ln(k), y-intercept [19]. The rate constant k is frequently evaluated from the half-time of crystallization, $t_{1/2}$, using $k = \ln(2)/t_{1/2}{}^n$ where n is the Avrami index since the intercept obtained by linear regression may not be statistically accurate.

2.3.2 Nonisothermal Crystallization

Crystallization of polymer melts, in practical processing operations, proceeds nonisothermally over a wide range of temperature. The general Avrami theory of phase change can be extended so as to describe nonisothermal crystallization kinetics. The overall crystallization rate constant, which contains contributions from nucleation and growth processes depends on the temperature, K = K (T). This is true of isothermal crystallization as well. It is assumed by most investigators studying nonisothermal crystallization that K is function of temperature only.

Nakamura et al. [21] expressed nonisothermal crystallization kinetics with the assumption of the isokinetic condition (i.e. ratio between nucleation rate and growth rate is constant independent of temperature) and independent of the ultimate crystallinity or the cooling process led to the following equation:

$$\frac{X(t)}{X_\infty} = 1 - \exp\left[-\left(\int_0^t K(T)dt\right)^n\right] \text{----------(2)}$$

where X(t) is the degree of phase transformation at time t, n is the Avrami index determined in the isothermal experiments, and K(T) is related to the isothermal crystallization rate through the relation $K(T) = k(T)^{1/n}$.

2.4 Melt Spinning Fundamentals

2.4.1 Crystallization Kinetics in Melt Spinning

Molecular orientation has a great influence on the rate of crystallization at a constant temperature in the melt spinning of polymeric materials. There have been few general formulas expressing the quantitative relation between the rate of crystallization

and molecular orientation with the difficulty caused by the extremely high crystallization rate [22, 23].

Polymer crystallization is closely related to molecular orientation in the amorphous regions, in addition to the temperature history through processing conditions. Under nonisothermal condition, the crystallization of a semicrystalline polymer almost always occurs preferably in the presence of molecular orientation. Observations of polymer crystallization in shear flow or in stirred polymer solutions confirm the importance of molecular orientation.

Many observations concerning polymer crystallization in elongational flow are indicative of the great importance of orientation effects in fiber formation.

Wasiak et al. [24] made a thorough study of crystallization and changes in amorphous and crystal orientation, using uncrosslinked samples of PET with various degrees of initial orientation. It was found that orientation of amorphous phase led to a substantial increase in crystallization rate and this effect, in turn, depended on the crystallization temperature: the higher the temperature, the stronger is the effect of orientation.

Nakamura et al. [25] observed that melt spinning of PET at low spinning speeds usually yields completely amorphous, glassy fibers due to the very low kinetic crystallizability of the polymer. But, high-speed spinning accompanied by strong molecular orientation, despite an increased cooling rate, produces partially crystalline fibers. This can only be explained when it is assumed that the increase in crystallization rate due to molecular orientation is so large that it could compensate for the effect of reduced crystallization time.

Ziabicki [26] was the first to consider the molecular orientation factor and determined the kinetic function of non-isothermal and oriented condition:

$$K(T,f) = K_0(T)\exp(A(T)\cdot f^2) \text{ ----------(3)}$$

where K_0 (T) is the crystallization rate in the isotropic and unoriented system, f is the orientation factor, and A(T) is a material constant dependent on temperature.

Katayama and Yoon [27] simulated the crystallization rate during the melt spinning. With the increase of molecular orientation, the rate constant k_A increases rapidly and the Avrami index n decreases to 1 or even below if crystallization kinetics is expressed by the Avrami equation. The generalized Avrami equation is expressed as:

$$X = 1-\exp\left[-\left(\int_0^t K(T(\tau),\Delta n)d\tau\right)^n\right] \text{ ----------(4)}$$

where K(T, Δn) is a crystallization constant depending on the temperature and orientation. They also suggested that the overall crystallization rate constant is a function of both temperature and molecular orientation and can be expressed by

$$K(T,f) = K_0\exp\left[-\frac{U^*}{R(T-T_\infty)}\right]\exp\left[-\frac{C_3}{T\Delta T + CT^2f^2}\right] \text{ ----------(5)}$$

where K_0 and C_3 can be obtained from quiescent isothermal crystallization kinetics data. The value of C_3 expresses the influence of the molecular orientation on the crystallization rate [27].

2.4.2 Modeling of the Melt Spinning Process

In the manufacture of PET fibers, melt spinning is the fundamental operation and the understanding of spinning dynamics has become the key point of the melt spinning.

The profile of the spinning line and the appearance of a neck-like deformation play an important role both in the development of internal structure and in the stability of the process. Elucidation of the effects of spinning speed, cooling, rheological properties of the polymer, and crystallization provides a critical condition for optimization of the spinning process.

A complete series of theoretical analysis and experimental investigation on the spinline dynamics, was first understood by the work of Ziabicki and Kedzierska [28] and the model described here is based on the early work of Kase and Matsuo [29] and the more recent models of George [30], Katayama and Yoon [27], Shimizu et al. [31], Zeminski and Spruiell [32] and Patel et al. [33].

(1) Mass balance

In a steady state spinning process,

$$W = \rho A V \text{ ----------} (6)$$

where W is the mass throughput per a spinneret hole, ρ is the filament density, A is the filament cross sectional area and V is the filament velocity.

(2) Momentum balance

The gradient of axial tension along the spinline results from several different contributions,

$$\frac{dF}{dz} = W\frac{dV}{dz} - \pi\sigma\frac{dR}{dz} - \rho g\pi R^2 + 2\pi R p_{xr,s} \text{ ----------} (7)$$

and after integration,

$$F(z) = F(0) + W(V - V_0) + \pi\sigma(R_0 - R) - \pi\sigma g\int_0^z R^2 dz + 2\pi\int_0^z R\tau_f dz \text{ ---------} (8)$$

where V is current axial velocity of the filament at the distance z from the spinneret; V_0 is the extrusion velocity; R and R_0 are current radius of the filament and radius of the orifice, respectively; σ is surface tension; ρ is polymer density; g is the acceleration of gravity; and τ_f is shear stress on the filament surface resulting from air drag, which causes a friction around the skin region of filament.

The individual terms in the above equation describe the contributions of rheological drag at z = 0, inertia, surface tension, gravity, and air drag forces, respectively.

$$F(x) = F_{rheo}(x) = F_{rheo}(0) + F_{in} + F_{surf} - F_{grav} + F_{air} \text{ ----------(9)}$$

More detailed analysis shows that the effects of surface tension, $F_{surf} = \pi\sigma(R_0 - R)$, and gravity, $F_{grav} = \pi\rho g \int R^2 dz$, are generally small compared to other terms and except for very slow spinning of thick filaments, they contribute less than 1% of the total tension and are negligible for both low and high speed spinning processes. Therefore, neglecting radial variations and the force due to surface tension with mass balance for a cylindrically shaped filament, $W = \rho\pi(D/2)^2 V$, changes the above equation as,

$$\frac{dF_{rheo}}{dz} = W\frac{dV}{dz} + \frac{1}{2}\rho_a C_d V_r^2 \pi D - \frac{Wg}{V} \text{ ----------(10)}$$

where ρ_a is the density of air, V_r is the relative axial velocity of the spinning filament and the cooling medium, and D is the filament diameter. C_d is the drag coefficient and is defined using the equation for the shear stress at fiber-air interface due to aerodynamic drag, $\sigma_f = 1/2\rho_a C_d V^2$.

(3) Energy balance

In nonisothermal melt spinning, an energy balance is required to determine the filament temperature as a function of distance or time from a spinneret.

Heat transfer from the spinline to the cooling medium provides another important velocity-dependent factor in melt spinning dynamics. Heat transfer in the spinning operation involves several mechanisms: radiation, free convection and forced convection.

Unlike the melt spinning of inorganic · glasses or metals, where extrusion temperatures are increased up to 900-1300 °C and, hence, the contribution of radiative heat transfer is considerable, the radiation contribution in the melt spinning of polymers can be usually neglected compared to the convective heat transfer since the extrusion temperatures in the polymer melt spinning are generally less than 300 °C.

For PET having a low crystallization rate, the effect of heat transfer caused by crystallization, is also negligible in the spinning speed from slow to moderate. High rates of crystallization, however, are obtained in PET when it is melt spun at high spinning speeds, which is attributed to the stress induced crystallization. This requires heat of crystallization should be considered in energy balance:

$$\frac{dT}{dz} = -\frac{\pi Dh(T - T_a)}{WC_p} + \frac{\Delta H_f}{C_p}\frac{dX}{dz} \qquad (11)$$

where T is the filament temperature, T_a is the temperature of the cooling medium, ΔH_f is the heat of fusion, X is the crystalline fraction, h is the heat transfer coefficient, and C_p is the polymer heat capacity.

(4) Constitutive equation

The axial stress in the spinline and the rheological force is related to the spinline kinematics through the rheological constitutive equation.

$$\eta\left(T,\dot{E}\right)=\sigma_{zz}/\left(\frac{dV}{dz}\right) \quad \text{----------(12)}$$

where η is defined as a uniaxial "apparent elongational viscosity", which may be a function of both temperature, T, and strain rate, $\dot{E}$, and σ_{zz} is the axial stress in the spinline.

The viscosity of most polymers changes greatly with temperature. The viscosity for Newtonian liquids and polymeric fluids generally follows the Arrhenius equation in high temperature range well above the melting temperature:

$$\eta = A\exp\left(\frac{B}{RT}\right) \quad \text{----------(13)}$$

where A is a characteristic of the polymer and its molecular weight at a given shear stress and B is the activation energy for the flow process.

For amorphous polymers, the Arrhenius equation does not fit the data well as the temperature approaches the glass transition temperature and it is advisable to shift to the Williams-Landell-Ferry (WLF) equation [34]:

$$\log_{10}\left(\frac{\eta}{\eta_g}\right)=\frac{-C_1\left(T-T_g\right)}{C_2+\left(T-T_g\right)}-\log_{10}\left(\frac{T_g\rho_g}{T\rho}\right) \quad \text{----------(14)}$$

where ρ_g is the density at the glass transition temperature, T_g. The second term in the right side, $\log_{10}\left(T_g\rho_g/T\rho\right)$ is almost zero and negligible. The Arrhenius equation is

generally satisfactory with the temperature range greater than (T_g+100 °C) whereas the WLF equation or similar type of equation at the low temperatures.

(5) Orientation development

Parallelization and extension of macromolecules and other structural units (crystallites, fibrils, etc.) along the fiber axis, usually referred to as molecular orientation, affects many physical properties of natural and man-made fibers such as tensile strength, modulus, sorption of solvents, optical and electrical behavior. On the other hand, the polymer crystallization, kinetics of solidification, and dynamics of deformation are significantly affected by the orientation development during the spinning or drawing process, which makes orientation play an important role in all fiber formation [35].

Polymers are considered to be in thermodynamic equilibrium with external stresses at temperatures well above the glass transition temperature, which means that there are no residual stresses possible. It has been noted that the birefringence, a measure of overall orientation, of a filament being spun from an amorphous polymer has a linear relation with the applied stress well above the glass transition temperature and at relatively low stress levels [36]:

$$\Delta n_{am} = C_{op}\sigma_{zz} \quad \text{----------(15)}$$

where $\Delta n = n_{11} - n_{22}$ is the difference of principal refractive indices between the directions of the stretch and perpendicular to it, and C_{op} is the stress-optical coefficient. This equation is valid only in the rubbery state where the stress rises from the change in entropy with elongation.

In the case of semicrystalline polymer, however, the situation becomes more complicated. It is assumed in this case that oriented crystal nuclei form in the oriented melt. Orientation-induced crystallization, therefore, proceeds on these oriented nuclei, producing additional relatively highly oriented material as the fraction of crystalline material increases. This typically increases the overall orientation and birefringence in the filament. Total birefringence in case of semicrystalline polymer can be expressed as [37]:

$$\Delta n = (1 - X_c)\Delta n_a + X_c f_c \Delta_c^0 + \Delta n_f \text{ ----------(16)}$$

where X_c is the crystalline fraction and the subscript c and a refer to the crystalline and amorphous phase, Δ_c^0 is the intrinsic birefringence of the crystalline phase, and f_c is the Herman's orientation factor for the crystalline phase. Δn_f is a form birefringence due to interaction of the two phases with light. This term is small enough to be neglected in case of semicrystalline homopolymer fibers.

2.4.3 Structure Development in Melt Spinning of PET

Synthetic fibers, such as polyesters and polyamides, are usually manufactured by melt spinning, where polymer is melted and extruded through a number of capillaries, and drawn-down to form filaments or fibers. Before the notion of high speed melt spinning was introduced, a conventional two-step process had been widely used: Yarn is melt spun at the speed of 1000~1500 m/min and taken up on a package and hence, the degree of orientation and crystallinity of yarn is relatively low in step 1. In step 2, in order to increase the mechanical and physical properties of the yarn melt spun at low spinning speeds of 400~1000 m/min, it is subjected to a drawing process [38].

Considerable technical effort has been devoted in order to increase the spinning speed and hence the productivity of PET fibers, since PET emerged as a commercially significant fiber forming polymer. From the industrial point of view, high speed spinning technology is attractive if the synthetic fibers are produced with as high degree of orientation and crystallinity as those fibers from two-step process, in that it can increase productivity by simplifying the process and therefore, reduces the total production cost.

PET exhibits, generally, a rather low crystallization rate, short relaxation time and low viscosity [39, 40, 41]. The rate of crystallization is sufficiently slow and the rate of cooling is high enough to prevent crystallization from occurring at low and moderate spinning speeds, below 3500 m/min. The fibers spun at these conditions exhibited an amorphous structure or a mesophase, oriented amorphous structure from the data of density, x-ray, DSC analysis and shrinkage measurements [42, 43]. It was suggested by Nakamura et al. [44] that PET would crystallize due to enhanced crystallization rate at high speed spinning and spinline stress conditions, which is apparently attributed to increased molecular orientation produced in the melt.

The conformation of fiber molecules determines the morphology of fiber structure and also highly oriented fiber molecules significantly influence the morphology of the fiber and its physical properties. There has been, therefore, persistent interest in research on high speed melt spinning with both theoretical and practical significance.

In 1952, Hebler [45] produced PET fibers at speeds in excess of 4700 m/min in which boiling water shrinkages of less than 4% were observed while low speed yarns exhibit shrinkages in excess of 30%. Ludewig [46] discusses some of the early PET

spinning studies, which deal with x-ray and tensile properties to show the presence of crystallinity.

There was little or no literature on this subject until Heuvel and Huisman [42] published their extensive x-ray studies in 1978. They have characterized as spun PET (Intrinsic Viscosity, I.V.=0.63) yarns produced at high speeds up to 6000 m/min. On the basis of density measurements, they found the onset of crystallization to occur between 3500 and 4000 m/min. They also present thermomechanical analysis (TMA) and found that the crystalline density increases from 1.488 g/cm^3 at the lowest speed with meaningful x-ray structure, 4750 m/min, to 1.501 g/cm^3 at 6000 m/min along with an increase in estimated crystallization temperature from 186 to 218 °C.

Shimizu et al. in a series of papers have studied the spinning of PET at speeds up to 9000 m/min. In the first paper [47], the density, x-ray, tensile, differential thermal analysis (DTA), and shrinkage data of as spun PET (I.V.=0.644) indicate the onset of the crystallization process occurring in the 3500~4500 m/min, which are generally in accord with the results of Heuvel and Huisman [42]. These authors report significantly higher crystallinity than Heuvel and Huisman, e.g., 40% vs. 24% at 6000 m/min and somewhat lower crystalline orientation factor, e.g., 0.91 vs. 0.98 at 6000 m/min. The variation in crystallinity observed may well not be real, but the result of using different assumed values of crystalline and amorphous densities.

An interesting observation reported by George and Ziabicki [48, 40] is that of all the orientation-related yarn properties reported, only birefringence fails to show clearly the transition from the essentially amorphous to partially crystalline state. A possible explanation of this is that total orientation increases continuously with spinning speed and

when sufficient orientation exists under proper conditions of temperature and stress, some of the material crystallizes without significantly changing the total orientation of the yarn.

Shimizu et al., in a subsequent paper [49], examine the effects of flow rate per hole over the speed range. The observed effects are small but consistently show that somewhat higher speeds are required to achieve a given level of crystallinity as flow rate is increased in the intermediate speed range, from 4000 to 5000 m/min.

In their third paper, Shimizu et al. [50] discuss the effects of molecular weight as measured by I.V. The results are consistent in showing that higher molecular weight crystallizes at lower speeds and they hypothesize that the increased viscosity of the higher molecular weight polymers leads to a higher spinline stress, which accelerate the orientation and crystallization. They continue to discuss yarns spun at speeds up to 9000 m/min and find some significant changes occurring above about 7000 m/min. Birefringence and density begin to decrease, while the crystallinity tends to level off. They see skin-core effect in differential birefringence suggesting that a significant radial temperature gradient is present during a critical phase of the structure development process and these effects are not seen to any great extent at speeds below 6000 m/min [51].

Shimizu et al. [52, 53] reported that the importance of spinline stresses, especially the air drag and inertia stress, is increased in high speed spinning with more weight on the inertia stress, and they also reported the effect of spinning speed on the unit cell parameters and superstructure of as spun PET fibers. The values of a, b and c show their minima around 7000 m/min and crystal density increases with increasing spinning speed in the range of 5000~7000 m/min and decrease above 7000 m/min. The crystallite sizes

in three lateral directions as well as in the chain direction increase monotonically with spinning speed, whereas the imperfection parameter along the chain axis decreases with the increase of spinning speed and is considerably smaller than for the lateral directions.

George [30] has developed a mathematical model of melt spinning of PET at speeds below 3500 m/min and a correlation between the stress at the freeze point (point along the spinline at which the filament reaches its final velocity) and the spun yarn birefringence. At low speeds below 3500 m/min, the model forces this point to occur at a spinline temperature equal to 70 °C, which is normally the glass transition temperature, T_g of amorphous PET. It has been summarized that there is a stress-supercooling interaction at intermediate velocities or stresses, which allows crystallization to occur at higher temperatures as stress increases and this interaction again breaks down with the observed supercooling being higher than predicted at high stresses.

George et al. [48] found that the freeze temperature increases with stress or windup speed and also that the shape of the velocity profile changes significantly. At low stress, the velocity profiles rise smoothly to the final velocity in fairly gradual manner. As the speed increases, this rise becomes more abrupt until at the higher speeds it essentially jumps from about 25% to 80 or 90% of the winder speed in a few centimeters, suggesting an almost instantaneous change from a viscous melt to a semicrystalline solid that is essentially nondeformable at the stress levels encountered on the spinline. This is consistent with the necking observed by Perez and Lecluse [54].

It is well known that the high speed melt spinning of crystallizing polymers is generally accompanied by abrupt diameter attenuation right above the solidification point in the spinline. This behavior is so similar to the necking phenomena frequently observed

in cold drawing that such a deformation in high speed melt spinning is referred to as a "necklike deformation." The control of the necking behavior leads to enhanced structure and properties of high speed spun fibers because the major structure development in fibers takes place within the necking zone in the spinline.

Perez and Lecluse [54] measured velocity and temperature profiles as well as extensive structural measurements and reported that orientation-induced crystallization occurs around the spinning speed, 3500 m/min, and at the spinning speeds in the neighborhood of 5000 m/min, the PET filaments exhibit a rapid draw-down or necking in the diameter profile along the spinline. They reported that the neck becomes more abrupt and more evident with increase in spinning speed above 4500 m/min and the birefringence rises abruptly at the point in the spinline at which the neck occurs. X-ray diffraction patterns on the samples containing necks show only amorphous halo above the neck. Just below the neck, however, the patterns exhibit crystalline reflection indicating a high degree of orientation and crystallization.

In 1982, Shimizu et al. [55] reported a sharp diameter thinning on the spinline at spinning speeds above 5000 m/min and have suggested that the viscosity decrease due to formation of an oriented mesomorphic phase, or as a result of some rheological change such as a decrease in viscosity with the increase in deformation rate which occurs in the spinline.

Kase [56] suggested that the cold-drawing theory is valid in the neck-like deformation in high speed melt spinning and that the necking behavior is due to the constitutive nature of the polymer. The necking behavior has also been discussed in terms of high Deborah number viscoelastic responses coupled with nonisothermal conditions

[57]. In addition to this approach, it was proposed that axial and radial viscosity variations could cause the necklike deformation in high speed melt spinning [58, 59]. There has been an attempt to treat the necklike deformation in high speed melt spinning as a problem of sensitivity to external disturbances [60].

The phenomenon of neck formation has attracted considerable attention, but it is not readily explained. When necking is observed, it is invariably associated with crystallization in the spinline, frequently occurring at a point on the spinline just before crystallization is detected. However, crystallization in the spinline is itself not a sufficient condition to cause necking, as numerous examples exist of crystallization occurring in the spinline without noticeable neck formation.

2.5 Poly(ethylene terephthalate) Copolymers

2.5.1 General Background

Modification of polyesters by the introduction of a third component has been widely practiced for obtaining properties differing from those of a two-component system [3]. Due to poor hygroscopicity and dyeability, attempts have been made to modify poly(ethylene terephthalate) by incorporating either long-chain diols or dicarboxylic acids [4~7]. However, the incorporation of comonomers leads to poor mechanical properties. Copolyesters with increased dyeability, moisture regain, and flame retardancy have also been produced by the introduction of alicyclic, substituted aryl, or aryalkyl diols as a third component.

Varma et al. [61] described the effect of structure on moisture regain and dye uptake of copolyester fibers of poly(ethylene terephthalate) and poly(hexamethylene terephthalate), poly(octamethylene terephthalte), and poly(decamethylene terephthalate).

They suggested that the increase in the methylene groups per repeat unit of copolyesters resulted in an increase in moisture regain and dye uptake. Sacak et al. [62] improved moisture regain by grafting vinyl monomer, acrylamide onto PET fibers, resulting in the increased moisture regain. They suggested that this increased moisture regain could be attributed to the hydrophilic nature of the grafted monomer and the structural changes due to grafting.

Hsiue et al. [63] investigated improving the thermal shrinkage of PET fibers by using poly(ethylene isophthalate terephthalate), which can be used for the application of thermal shrinkage packing materials. They suggested that the chains of the copoly(ethylene isophthalate terephthalate) are oriented more loosely that those of the PET and the copolyesters have more amorphous regions, which result in the increase of the thermal shrinkage.

Datye et al. [64] modified the unfavorable alkali hydrolysis property of PET by incorporating dihydroxyethyl-5-sulfoisophthalte and Kiyotsukuri et al. [65] also suggested that resistance to alkali hydrolysis could be enhanced in PET copolyesters by using poly(butylenes glycol) as a third comonomer.

2.5.2 Crystalline Part of Copolymers

For the crystalline part of a copolymer, it can be assumed two cases. One is the case of a mixed crystal system where both A and B cocomponents coexist in its crystalline parts, and the other is the case in which the crystals consist of only one of the cocomponents (A component). In the latter case, P. J. Flory [13] showed that the following equation could be derived for the relationship between the theoretical melting point of a copolymer and its composition:

$$\frac{1}{T_m}-\frac{1}{T_m^0}=-\left(\frac{R}{\Delta H_u}\right)\ln N_A=\left(\frac{R}{\Delta H_u}\right)\ln p \quad \text{----------(17)}$$

where T_m is the melting point of a copolymer, T_m^0 is the melting point of a homopolymer which consists of only an A component, ΔH_u is the heat of fusion of homopolymer crystals which consist of only an A component, p is the sequence propagation probability which corresponds to the molar fraction of A component, N_A, in the case of an ideal random copolymer, and R is the gas constant.

2.5.3 Amorphous Part of Copolymers

A glass transition temperature is defined as a temperature at which amorphous parts transfer from the glassy state to the rubbery, which hence can be regarded as a measure of flexibility of molecular chains. Since the early work of Gordon and Taylor [66], there have been many theoretical studies [67, 68, 69] on the variation of the glass transition temperature of copolymers with the copolymer composition. In the case of copolyesters, Gordon-Taylor's equation or Wood's equation was followed when the measurements of glass transition temperature were carried out on a specimen which was quickly quenched from its molten state, without any crystallization. Although the theories are based on the different assumptions, both can be represented by Wood's equation [68]:

$$T_g=\frac{\left[T_{g_1}+\left(KT_{g_2}-T_{g_1}\right)C_2\right]}{\left[1-\left(1-K\right)C_2\right]} \quad \text{----------(18)}$$

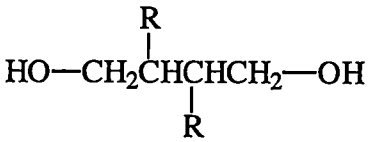
where T_g, T_{g_1} and T_{g_2} are the glass transition temperatures of the copolymer, the homopolymers formed from components 1 and 2, respectively, K is a characteristic constant for the constituent, and C_2 is a function of component 2.

2.5.3 Properties of PET Copolymers

Gordon and Mera [70] reported PET copolymers with 2,3-dialky-1,4-butanediols, where the dialkyl groups are longer than butyl, as shown in **Figure 2.3**, and studied the effect of varying length and amount of long alkyl side chains on inherent viscosity, and thermal behavior (glass transition temperature, melting and side-chain crystallization). They showed that the alkyl distributed butanediol comonomer contents in the products are smaller than those in the feeds, which is explained by the hydration and cyclization of alkyl-disubstituted butanediol to 2,3-dialkyltetrahydrofuranes during polyesterification. The inherent viscosity remarkably decreased with increasing content of alkyl disubstituted butanediol. The glass transition temperature decreased with increasing length and amount of alkyl side chains. Longer alkyl side chain gave rise to less depression of melting point and melting peaks from side-chain crystallization were observed at 11 and 34 °C for copolymer with alkyl side chains containing sixteen and nineteen carbon atoms, respectively.

Kiyotsukuri et al. [65] used another approach for copolymerization of alkyl disubstituted aliphatic diols. They used 2,2-dialkyl-1,3-propanediols with the alkyl side group shorter than butyl group as a third comonomer, as shown in **Figure 2.4**. They suggests that the 2,2-substituted short alkyl side group in propanediol hardly affects the reactivity of polymerization, whereas 2,3-disubstituted long alkyl side groups in butanediols remarkably decreased the inherent viscosities of copolymers shown by Gordon and Mera [70].

Kiyotsukuri et al. [65] found that all copolymers did not crystallize during the film preparation process and both crystallinity and density decrease with increasing



R = CH_3

$(CH_2)_4CH_3$

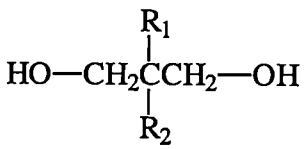
$(CH_2)_2CH(CH_3)_2$

$(CH_2)_{12}CH_3$

$(CH_2)_{15}CH_3$

$(CH_2)_{18}CH_3$

Figure 2.3 Chemical structures of 2,3-dialkyl-1,4-butanediols.



R_1	R_2	Code
H	H	HH
CH_3	CH_3	CC
C_2H_5	C_2H_5	C_2C_2
C_2H_5	C_4H_9	C_2C_4

Figure 2.4 Chemical structures and codes of 2,2-dialkyl-1,3-propanediols.

content of comonomer and length of the alkyl side chain in the comonomer, which can be attributed to considerably suppressed crystallization of PET chains caused by the increase of steric hindrance due to the longer alkyl side chains. From thermal analysis, they found that glass transition temperature decreases, cold crystallization temperature increases and melting temperature decreases with increasing content of comonomers and length of alkyl side chain. The peaks at both cold crystallization and melting temperatures, disappear at a comonomer content in the feed above 20 mole% for C_2C_2 and C_2C_4 copolymers, suggesting that these copolymers do not crystallize during the heating run of the thermal analysis. Tensile strength and elongation are increased and the Young's modulus decreased with the increase of comonomer content. They suggested that the alkyl side chain may disturb the interaction and cohesion of the polymer chain, which leads to the increase of extensibility of the polymer chain, and thus increases the tensile strength and elongation and decreases the Young's modulus.

Chen et al. [71] prepared PET copolymers with MPDiol and investigated the effect of the different MPDiol contents. They obtained similar results with those of Kiyotsukuri et al. [65], which is attributed to the similarities in the chemical structure of a third comonomer.

CHAPTER 3

MATERIALS, PROCESSING AND CHARACTERIZATION

3.1 Materials

A PET homopolymer (control) and four copolymers were prepared and supplied by Wellman, Inc. The copolymers had nominal (feed) compositions of 4,7,10 and 25 mol% MPDiol substituted for the ethylene glycol moiety in PET. A check on the compositions by NMR technique gave slightly higher MPDiol content in each case (5, 9, 12, 33 mol%), but the correlation was good and it was decided to use the nominal compositions in describing the results of our experiments. All resins were supplied as pellets with an intrinsic viscosity of 0.61 ±0.01 dl/g.

3.2 Processing

3.2.1 Melt Spinning Procedure

Prior to melt spinning, the resins were dried by heating under modest vacuum for 8 hours at 110°C (10 hours for the 25 mol% copolymer). Filaments were spun using the same equipment used in earlier studies from our laboratory [72~78]; the reader is referred to these articles for more detail. The melt spinning experiments were performed using a screw extruder supplied by Fourne Associates of West Germany equipped with a constant displacement melt pump that provided a constant extrusion rate.

The PET homopolymer and all MPDiol substituted copolymers, except the 25 mol% MPDiol resin, were spun with the same temperature settings -- the temperatures of zone 1, 2, 3 and 4 (spinneret) in the extruder were 273, 295, 280 and 265 °C, respectively. The settings for the 25 mol% MPDiol copolymer were 210, 280, 280 and 265 °C.

Molten polymer, supplied by the melt pump, was forced through a filter mesh and then through either a four-hole or single-hole spinneret with capillary diameters of 0.762 mm and L/D = 5.0. Using the four-hole spinneret, filaments were spun with total mass throughputs for all four holes ranging from approximately 2.5 g/min to 12 g/min (0.625-3.0 g/min/hole). The mass throughput for filaments spun with the single-hole spinneret ranged from about 2.15, g/min/hole to 8.25 g/min/hole.

Filaments spun at speeds below about 1200 m/min were wound directly onto a 6-inch diameter bobbin using a Lessona winder. At higher spinning speeds, two different methods were used for drawing down and collecting the filaments from the extruder.

In preliminary experiments, the filaments exiting the die were drawn down using an air-jet draw-down device. Air pressure applied to the device produces high-speed air, which provides a drag force to draw the filaments down. The amount of drag, and hence the take-up velocity of the filament, can be controlled by varying the air pressure supplied to the draw-down device. Depending on the viscosity of the polymer, spinning speeds up to about 5000 m/min could be obtained with air pressures up to about 80 psig. The distance from the spinneret to the spinline draw down device was kept constant at 2.5 m (250 cm).

In later experiments, the PET homopolymer and all copolymers, except the 25 mol% MPDiol resin, were spun at take-up velocities from 1000 m/min to their maximum spinning speeds by winding directly onto a 6.25-inch diameter godet. This godet could be rotated up to 12000 rpm, corresponding to a linear speed of 6000 m/min. In this case, the spinline length was kept constant at 3.5 m (350 cm).

The take-up velocities were determined by using the continuity equation shown in equation (6), assuming a steady-state spinning process. It is important to note that this method of determining the take-up velocity underestimates the actual take-up velocity due to change of filament diameter when the filament is allowed to relax. However, it is believed that this effect is similar for all the resins and should not have an appreciable effect on the comparisons made.

3.2.2 Post-Spinning Procedure - Drawing

The PET homopolymer and PET copolymers containing 4, 7 and 10 mol% MPDiol, were melt spun using a single-hole spinneret with a mass throughput of 8.25 g/min/hole and take-up velocities of approximately 600 and 1000 m/min. These melt spun filaments were then drawn using a Fincor 2-stage continuous drawing machine. In order to prevent filament breakage right after the bobbin, it was necessary to provide a preliminary heating before the first hot drawing godet. A schematic drawing of the post-spinning procedure is illustrated in **Figure 3.1**:

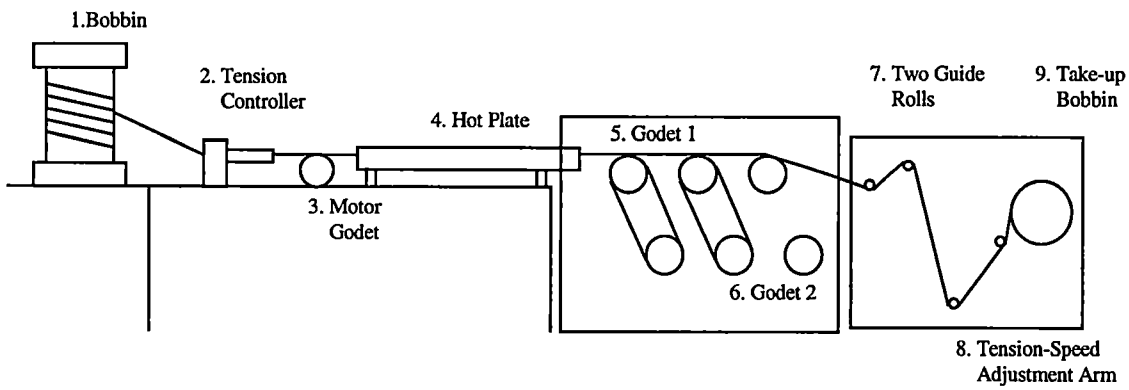


Figure 3.1 Schematic of the system used for post-spinning drawing.

The filaments had the following path along the drawing machine: (1) bobbin, (2) tension control device, (3) motorized godet to pull the filaments from the bobbin, (4) hot plate for first stage heating, (5) first godet that provides a first stage draw, (6) second godet that provides the second stage draw, (7) guide roll, (8) tension-speed control device, and (9) take-up bobbin for the drawn filament.

The speed of the motorized godet was kept constant at about one-third that of the first roll. This provided a first stage draw and prevented the filaments from sticking to the sides of the hot plate channel. The temperature of the hot plate channel was varied over a small range for each composition, but it was always chosen to be a bit higher than the glass transition temperature of PET. The temperature of the first godet was always chosen to be a bit higher than that of the hot plate, while the temperature of the second godet was maintained at ambient temperature. Temperature conditions for drawing are shown below in **Table 3.1**.

Table 3.1 Temperatures used for the drawing process.

Material	$T_{hot\ plate}$ (°C)	$T_{roll\ 1}$ (°C)	$T_{roll\ 2}$ (°C)
0 mole% MPDiol (PET)	80	90	Maintained at 25 °C
4 mole% MPDiol	80	110	
7 mole% MPDiol	85	95	
10 mole% MPDiol	85	110	
	90	100	
	90	110	

The draw ratios (DR) were determined from the equation

$$Draw\,Ratio\,(DR) = \frac{W_0}{W_f} \text{----------(19)}$$

where W_o is the weight in grams of one meter of fiber before drawing and W_f is the weight in grams of one meter of fiber after drawing.

3.3 Filament Characterization

3.3.1 Optical Birefringence

Light entering an isotropic crystal is refracted at a constant angle and passes through the crystal at a single velocity without being polarized by interaction with the electronic components of the crystal lattice. When light enters the optical axis of anisotropic crystals like polymers, it acts in a manner similar to interaction with isotropic crystals and passes through at a single velocity. However, when light enters a non-equivalent axis, it is refracted into two rays each polarized with their vibration directions oriented at right angles to one another, and traveling at different velocities. This phenomenon is termed birefringence and is seen to a greater or lesser degree in all anisotropic crystals.

Birefringence can be defined as the difference in the refractive indices of perpendicular directions as measured with light polarized along these respective directions, as shown in equation (20). Molecular orientation will in general give rise to non-zero birefringence. The measurements of how the birefringence changes with respect to a reference axis gives an indication of how the molecular chains are orienting.

$$\Delta n = n_{II} - n_{\perp} = \Gamma / d \text{----------(20)}$$

where $n_{\parallel}$, $n_{\perp}$ are the parallel and perpendicular refractive indices, respectively, Γ is the retardation value, and d is the fiber diameter.

Fiber birefringence was measured using an Olympus polarizing microscope, with a Leitz 10 or 30 order Berek compensator. A camera was attached to the microscope and measuring the diameter on a TV monitor and calibrating it with a 0.01 mm-graduated glass slide measured the diameter of a single fiber. The retardation of a fiber was calculated by using a table supplied by the Leitz compensator manual and birefringence of the fiber was determined by dividing the calculated retardation by the fiber diameter.

3.3.2 Differential Scanning Calorimetry (DSC)

The degree of crystallinity was determined using a Perkin-Elmer DSC-7 differential scanning calorimeter using an intercooler and nitrogen gas purge. Equipment calibration was performed periodically using an indium standard (ΔH = 28.45 J/g; T_m (onset) = 156.61°C). Test runs involved heating from 50 -290°C at a scanning rate of 10 °C/min. Although each test run was normalized to the sample mass, care was taken to ensure that the mass of each sample remained fairly consistent (5-7 mg) in order to pursue data precision.

The degree of crystallinity for each sample was found by subtracting the enthalpy of crystallization from the enthalpy of melting and dividing the difference by the specific heat of melting for PET ($\Delta H_{c,\,PET}$ = 140 J/g) [79]:

$$\%X = \left[\frac{|\Delta H_m| - |\Delta H_c|}{140}\right]100 \text{ ----------(21)}$$

3.3.3 Shrinkage in Boiling Water

Shrinkage gives an approximate indication of the degree of amorphous orientation. The higher the shrinkage, the higher is the orientation of amorphous regions since the shrinkage is the phenomenon of a polymer, of which amorphous region coils up with the introduction of a thermal energy.

The filament shrinkage was measured in boiling water. Filament sections a few centimeters long were immersed in the boiling water for 180 seconds. The %Shrinkage was calculated from the following equation with the averages of three sample measurements:

$$\%Shrinkage = \left(\frac{L_i - L_f}{L_i} \right) 100 \text{----------(22)}$$

where L_i is the initial sample length (before shrinkage) and L_f is the final sample length (after shrinkage).

3.3.4 Tensile Analysis

Tensile properties of filament samples were measured at room temperature on a Table Model 1122 Instron tensile tester using a gauge length of 25 mm, a constant crosshead speed of 50 mm/min, and a 500 g load cell. Six filament specimens from each sample were tested to break and the properties averaged. The tenacity and %strain at break from engineering stress-strain curves were determined using computer software supplied by the vendor.

3.3.5 Wide Angle X-ray Diffraction (WAXD)

Wide angle X-ray diffraction (WAXD) flat plate patterns were used to compare the relative crystalllinity and orientation of the crystalline phase in the filaments. WAXD patterns show amorphous "halos" from the amorphous phase and sharp reflections from the crystalline phase. Changes in the relative amounts of scattering from the amorphous and crystalline phases serve as a qualitative indicator of the relative amounts of crystalline and amorphous phases present in the filaments as a function of take-up velocity, mass throughput and MPDiol composition.

A Philips Norelco x-ray generator with nickel filtered CuK_α radiation of wavelength of 1.542 Å and a flat plate camera were used to determine wide angle x-ray scattering patterns of the filaments. The x-ray unit was operated at 40 kV and 15 mA with an exposure for 8 hrs. Crystalline orientation was judged based on the azimutal arc length of the crystalline reflections with a Bragg's law, $n\lambda = 2d_{hkl}\sin\theta$, as illustrated in **Figure 3.2.**

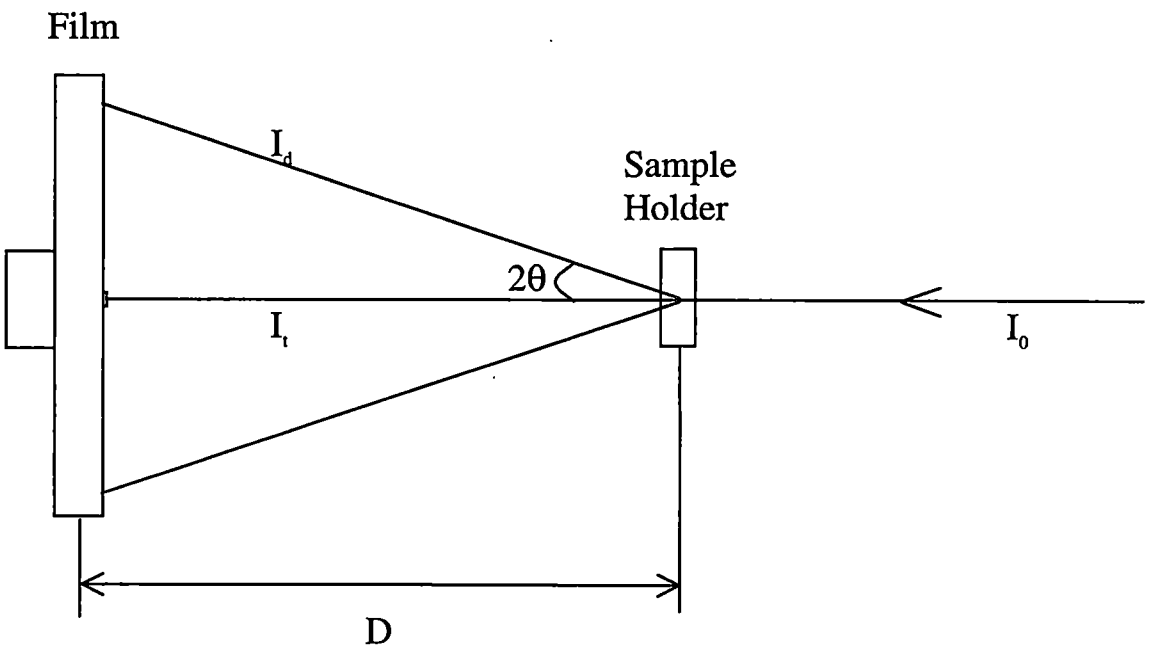


Figure 3.2 Schematic of wide angle x-ray diffraction (WAXD) unit, where I_0, I_t and I_d are the incident, transmitted and diffracted intensities, respectively.

CHAPTER 4

RESULTS AND DISCUSSION

4.1 Melt Spun Filaments Prepared with Air Drag Device

As noted above, two methods were used to draw the filaments down during the melt spinning process. In this section we describe the characteristics of melt spun filaments prepared using the air drag draw-down device.

4.1.1 DSC Crystallinity

Our DSC crystallinity measurements indicate that increasing the percentage of the MPDiol comonomer lowers the crystallinity of the melt spun filaments. This is illustrated in **Figure 4.1** for filaments spun with a mass throughput of approximately 8.5 g/min (2.1 g/min/hole). The actual mass throughput for each resin is also shown in the legend of **Figure 4.1**. The PET homopolymer filaments exhibit the well-known increase of crystallinity with take-up velocity caused by stress-induced crystallization. Except for the 25 mol% MPDiol filaments, the crystallinity of the other resins also increased as take-up velocity increased, but a lower crystallinity level than for the PET homopolymer. Within our ability to make the measurements, the 25 mol% MPDiol samples showed virtually no crystallinity at any take-up velocity. At the same take-up velocity, the crystallinity decreases with the increase of MPDiol content. This probably results from the MPDiol being unable to be incorporated into the PET crystal structure. The process of sorting through the polymer segments and rejecting the MPDiol units would be expected to reduce the rate of crystallization and lower the ultimate crystallinity that is obtained.

Figure 4.2 shows a plot of crystallinity versus take-up velocity for two PET homopolymers with different mass throughputs of 8.6 g/min/4holes (2.15 g/min/hole) and

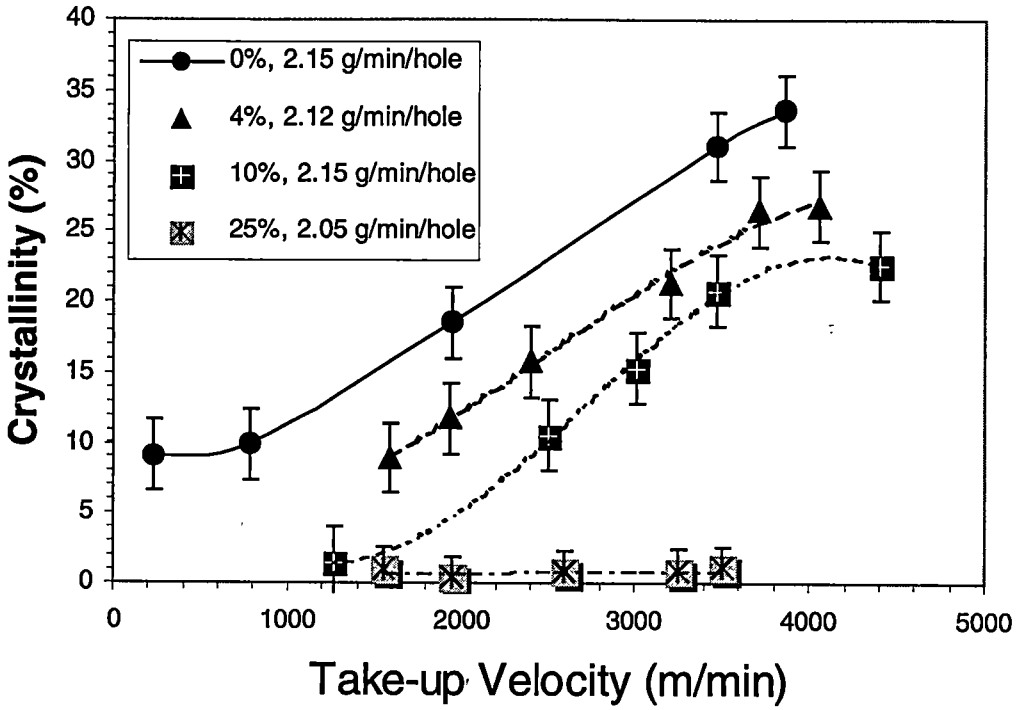


Figure 4.1 Crystallinity of air drag spun filaments prepared with a nominal mass throughput of around 2.1 g/min/hole.

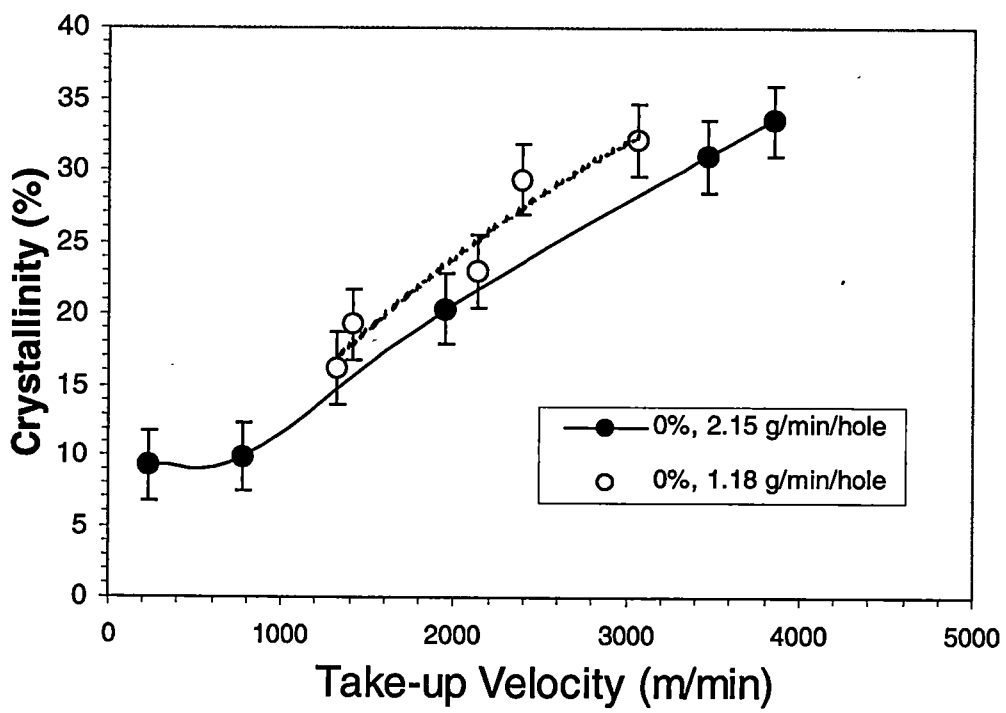


Figure 4.2 Comparison of crystallinity of PET filaments spun at two different mass throughputs.

4.7 g/min/4holes (1.18 g/min/hole), respectively. The plot of lower mass throughput shows a bit higher crystallinity than the higher mass throughput one, which can be explained on the basis that cooling rate in the spinline is faster for the lower mass throughput. This leads to an increase of spinline stress and molecular orientation in the filaments spun with the lower mass throughput at any given spinning speed. This, in turn, results in greater stress-induced (molecular orientation enhanced) crystallization.

It is noteworthy that higher cooling rate in the absence of molecular orientation enhanced crystallization would be expected to lower crystallinity rather than increase it, due to the shorter time available for crystallization in the appropriate temperature range. The fact that crystallinity increases with a decrease in cooling rate is therefore clearly associated with the influence of molecular orientation on the crystallization kinetics.

4.1.2 Optical Birefringence

The birefringence as a function of take-up velocity is shown in **Figure 4.3** for filaments spun with the air drag draw-down device. The error bars shown for PET are also representative of the errors in the other data. Note that the birefringence of all the resins is the same, within experimental error, up to a take-up velocity of about 2500 m/min.

The birefringence of the PET homopolymer exhibits an increase in the slope of the curve, starting at about 2500 m/min. This significant increase in the slope of the birefringence versus take-up velocity curve is associated with the development of significant stress-induced crystallinity. Below about 2500 m/min oriented crystals do not contribute significantly to the birefringence. However, above this take-up velocity,

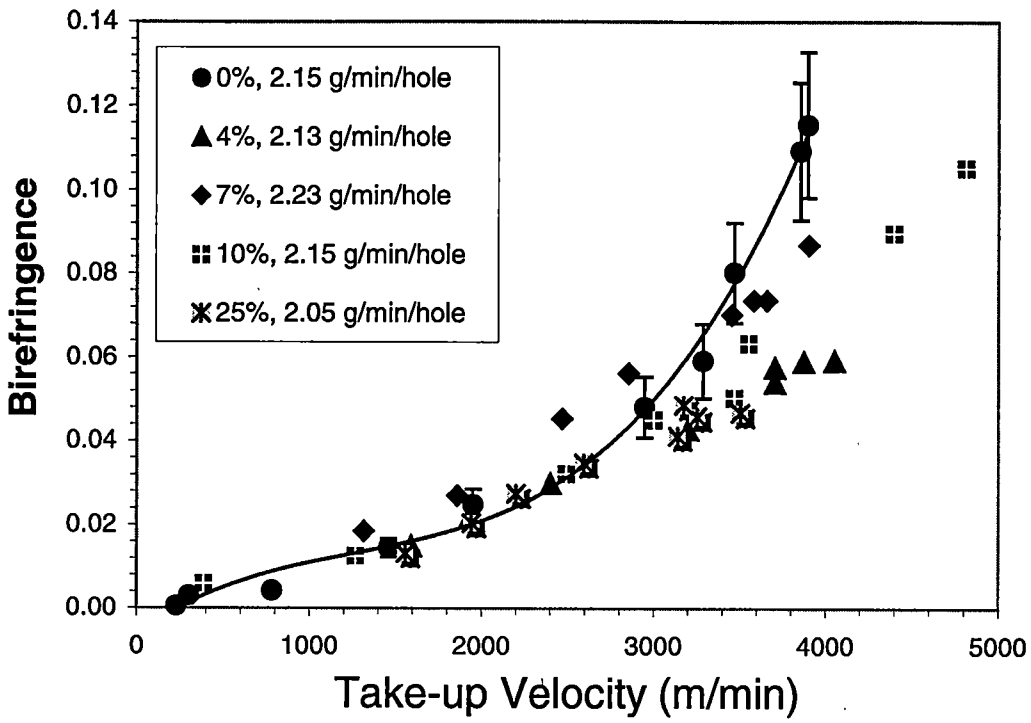


Figure 4.3 Birefringence of air drag spun filaments prepared with a nominal mass throughput of 2.1 g/min/hole (8.6 g/min/4holes).

oriented crystal nucleation and growth contribute greatly to the overall orientation measured by the filament birefringence. This interpretation is consistent with the literature for PET [42, 43] and with the present data for the 25 mol% MPDiol resin which exhibits no appreciable crystallinity and does not exhibit the noticeable change in slope exhibited by the PET homopolymer.

The data for the other resins lie between the data for the PET homopolymer and the 25 mol% MPDiol resin, although they do not exhibit the expected trend with composition. It is clear, however, that the 10 mol% MPDiol resin exhibits the effects of a lower level of crystallization. **Figure 4.4** shows a plot of birefringence versus take-up velocity for PET homopolymer and the MPDiol substituted filaments that were spun at a lower mass throughput, in the neighborhood of 5 g/min/4holes (1.25 g/min/hole).

These data indicate that the birefringence increases a bit more rapidly with take-up velocity at this mass throughput than at the higher throughput of **Figure 4.3**. Note, however, that at this low mass throughput, the maximum take-up velocities are substantially lower than for the higher mass throughput of **Figure 4.3** (except for the 25 mol% MPDiol resin). This is a result of the increased spinline stress caused by decreased melt flow rate, which increases the fiber orientation. The birefringence of the 25 mol% MPDiol substituted resin shows no appreciable increase beyond a take-up velocity of about 3500 m/min.

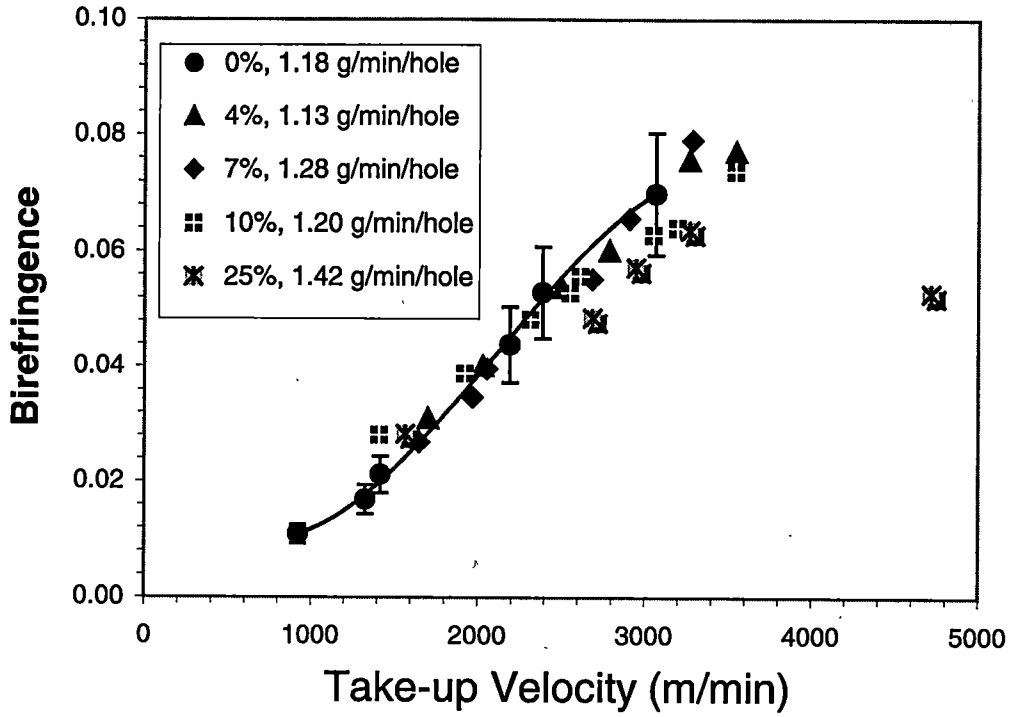


Figure 4.4 Birefringence of air drag spun filaments prepared with a nominal mass throughput of 1.25 g/min/hole (5 g/min/4holes).

4.2 Filaments Wound on a Godet

In this section, the characteristics of the filaments, except 25 mol% resin, prepared using a 6.25-inch diameter godet were determined and compared with those filaments prepared with air drag draw-down device.

4.2.1 DSC Crystallinity

DSC crystallinity of the filaments wound on a 6.25-inch godet showed a similar increase of crystallinity with the increase of the take-up velocities for PET homopolymer and MPDiol substituted PET copolymers as those filaments prepared with the air-drag device. As illustrated in **Figure 4.5**, however, it is noteworthy that the increasing percentage of MPDiol comonomer lowers the overall crystallinity over the range of take-up velocities and it also shifted the substantial development of crystallization to the higher take-up velocities, which is attributed to the lower crystallization rate caused by the introduction of more MPDiol comonomer content. In case of the measurements of filaments wound on a godet, the correlation between the degree of crystallinity and the content of MPDiol comonomer shows better-developed one than that of filaments prepared with the air drag device.

Figure 4.6 also illustrates the effect of the different mass throughputs in the crystallinity in PET homopolymer and 10 mol% MPDiol PET. As observed in air drag filaments, the lower mass throughput samples show higher crystallinity caused by the higher spinline stress, in both PET homopolymer and 10 mol% MPDiol PET. The difference in crystallinity is more obvious around moderate take-up velocity, below 3000 m/min, than that in the high take-up velocity above 4500 m/min. This is because

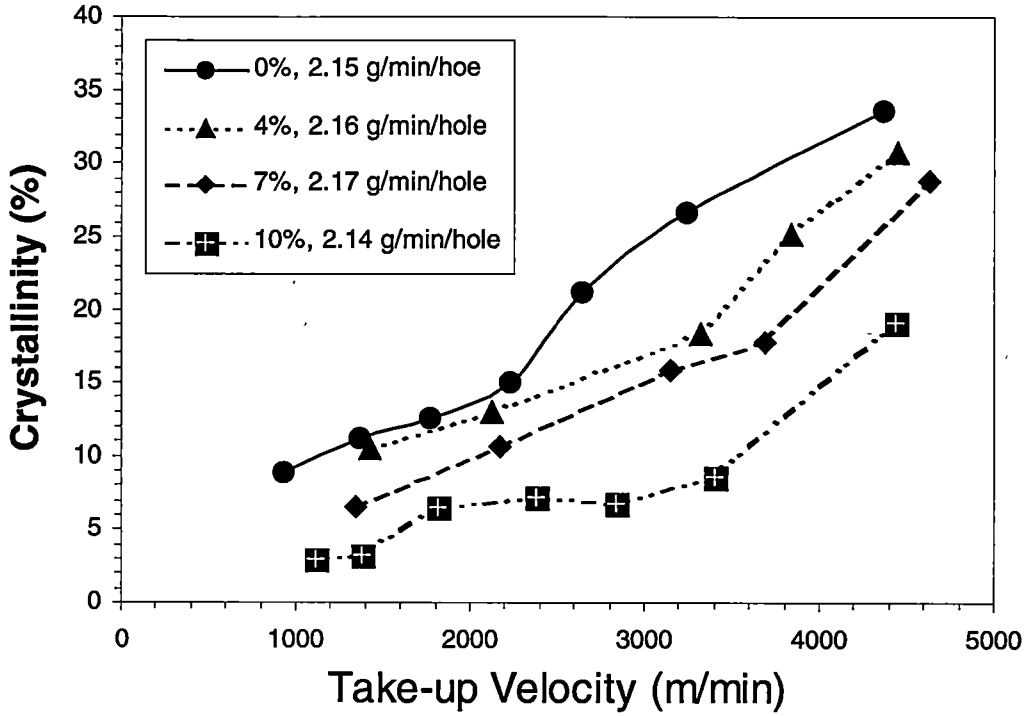


Figure 4.5 Crystallinity of filaments wound on a 6.25-inch diameter godet with a mass throughput of 2.15 g/min/hole.

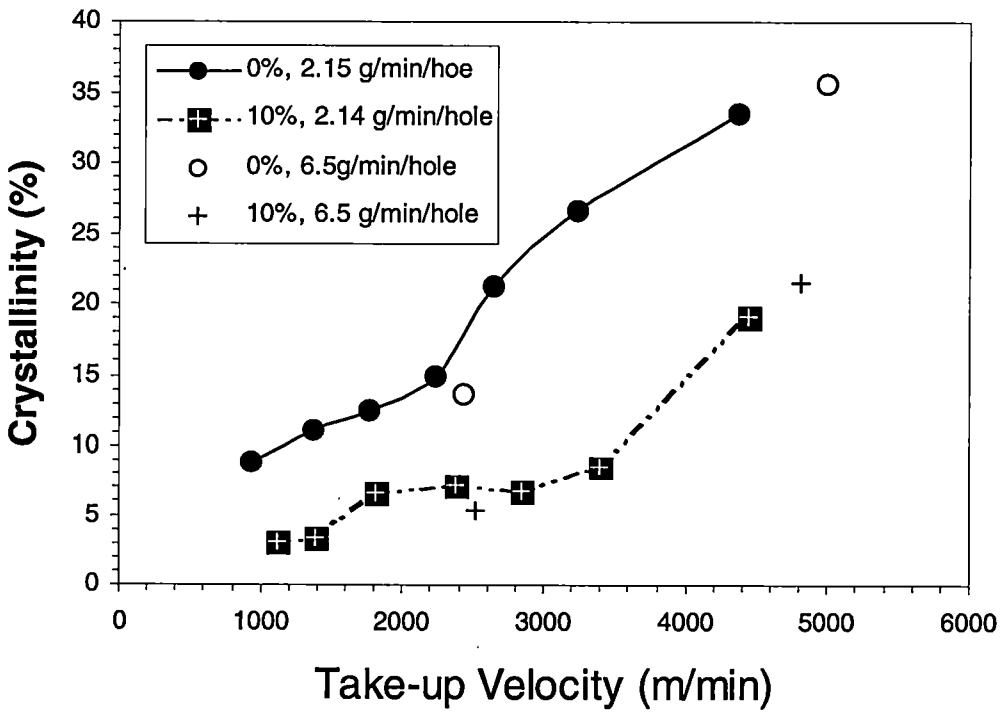


Figure 4.6 Comparison of crystallinity between two different mass throughputs of PET homopolymer and 10 mol% MPDiol PET copolymer.

molecular orientation induced crystallizations in the filaments of both lower and higher mass throughputs are well achieved in high take-up velocity.

4.2.2 Optical Birefringence

The birefringence of filaments spun using a godet take-up device with a mass throughput of about 2.15 g/min/hole are presented in **Figure 4.7**. Note that these filaments were spun as monofilaments (single hole spinneret) with a longer spinline (3.5 m versus 2.5 m) than for the filaments spun with the air drag draw-down device.

Note that the data of **Figure 4.7** exhibits somewhat less scatter and is more consistent with respect to the expected trend with the increase of MPDiol composition. This suggests that using the godet to draw the filaments down, together with a longer spinline, results in a more stable process. This is not surprising as the air drag draw-down is known to produce greater fluctuation in the spinning speed than a highly controlled godet. The general behavior of Figure 4 is still present, in that the PET homopolymer data rises more rapidly than the data for the copolymers in the region above about 2500 m/min.

Figure 4.8 shows the birefringence of filaments spun at a higher mass throughput of about 6.5 g/min/hole. The birefringence values rise a bit more slowly with take-up velocity at the higher mass throughput. This is attributed to the decrease of spinline stress due to slower cooling of the higher mass throughput.

4.2.3 WAXD Patterns

Flat plate X-ray patterns were made of filaments prepared from the PET homopolymer, 4 mol% MPDiol and 10 mol% MPDiol. These patterns provide a

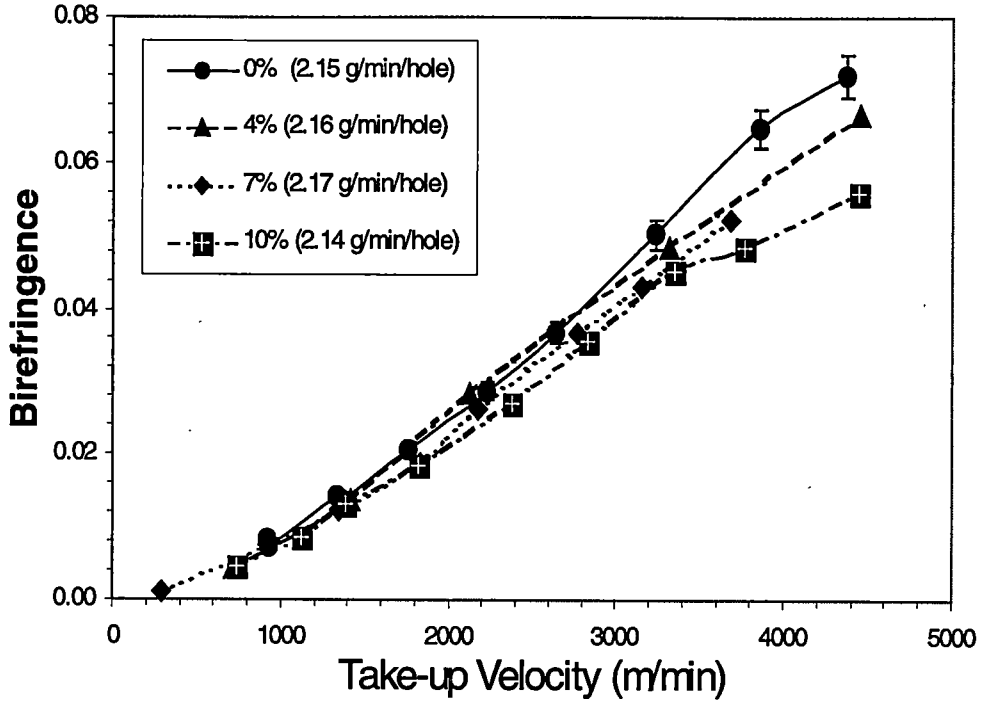


Figure 4.7 Birefringence of filaments spun with a godet draw-down and a nominal mass throughput of 2.15 g/min/hole.

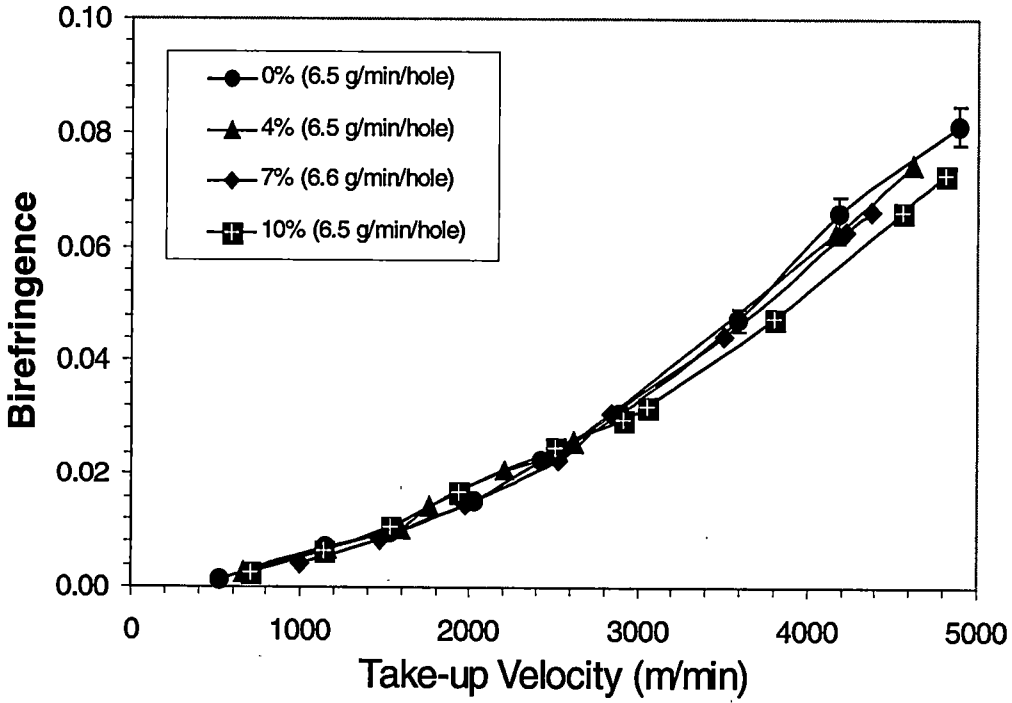
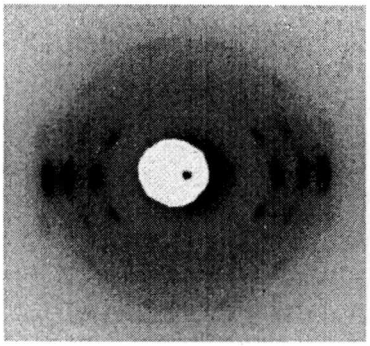


Figure 4.8 Birefringence of filaments spun with a godet draw-down and a nominal mass throughput of 6.5 g/min/hole.

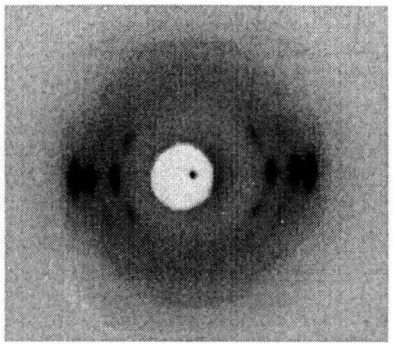
qualitative measure of orientation and crystallinity for comparison to the values of birefringence and DSC crystallinity. **Figure 4.9** shows patterns of selected filaments.

Crystallinity is barely detectable in the PET homopolymer at a take-up velocity of 2,230 m/min and a mass throughput of 2.15 g/min/hole. At the same mass throughput, the crystallinity and crystalline orientation of the PET homopolymer are well developed at a take-up velocity of 4,370 m/min. Likewise, at the higher mass throughput of 6.5 g/min/hole, the PET homopolymer has developed high crystallinity and crystalline orientation.

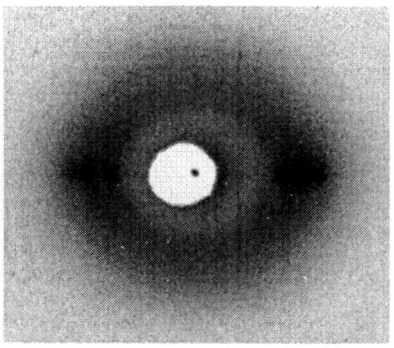
Note, however, that at similar take-up velocities and mass throughputs, the 10 mol% MPDiol filaments exhibit substantially lower crystallinity. These results are in general agreement with the results of the birefringence and DSC crystallinity measurements (**Figures 4.5, 4.6, 4.7 and 4.8**). At the lower take-up velocities, only amorphous halos could be seen, which is attributed to the low degree of orientation and negligible crystallization. With increase of take-up velocities, the amorphous halos first become more concentrated on the equator indicating improved orientation of the molecules. For PET homopolymer and 4 mol% MPDiol filaments, sharp crystalline reflections appear at about 2500 m/min and increase in intensity as take-up velocity increases further. In the case of 10 mol% MPDiol substituted PET, however, the flat plate patterns didn't show spots as sharp as those of 0 and 4 mol% PET. This result correlates well with the DSC results of **Figures 4.1, 4.5 and 4.6** that show a low level of crystallinity developed in the 10 mol% MPDiol containing filaments.



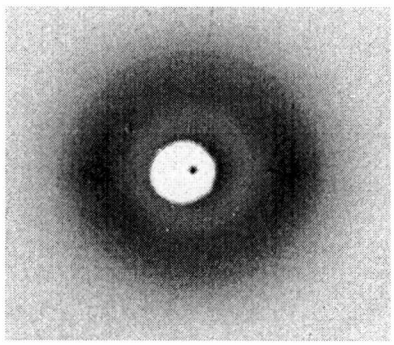
0 mol% MPDiol
2.15 g/min/hole
4,370 m/min



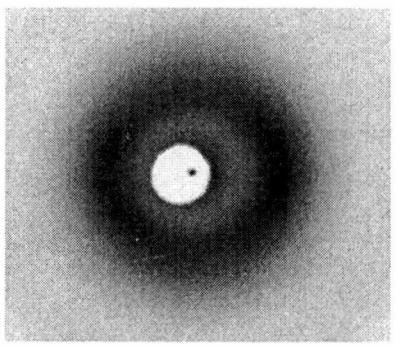
4 mol% MPDiol
2.16 g/min/hole
4,449 m/min



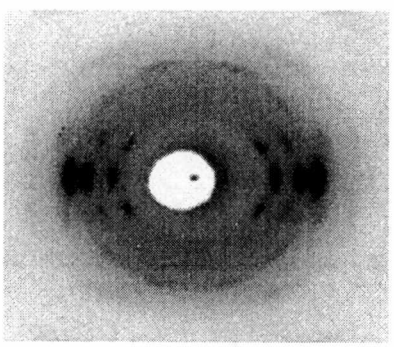
10 mol% MPDiol
2.14 g/min/hole
4,442 m/min



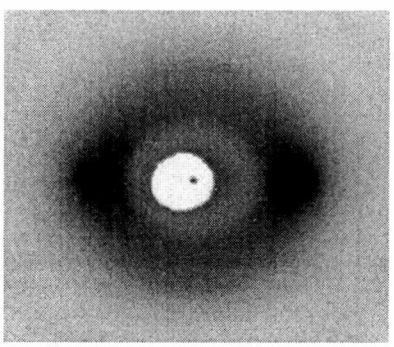
0 mol% MPDiol
2.15 g/min/hole
2,230 m/min



10 mol% MPDiol
2.14 g/min/hole
2,378 m/min



0 mol% MPDiol
6.5 g/min/hole
4,888 m/min



10 mol% MPDiol
6.5 g/min/hole
4,812 m/min

Figure 4.9 X-ray patterns of selected filaments at the indicated take-up velocities and mass throughputs.

4.2.4 Shrinkage

Shrinkage in boiling water for the filaments spun at a mass throughput of about 2.15 g/min/hole is shown in **Figure 4.10**. All data except for the 25 mol% MPDiol resin are for filaments prepared using the godet to draw the filaments down. At low spinning speeds the shrinkage increases due to the increase in the molecular orientation with increased spinning speed. The orientation is frozen-in below the glass transition temperature, but relaxes out, producing the shrinkage, when the filaments are heated in boiling water. At higher spinning speeds, the development of crystallinity tends to stabilize the filaments and reduce the shrinkage for all filaments except the 25 mol% MPDiol composition, which does not develop measurable crystallinity. As the level of crystallinity developed in the filaments increases, the shrinkage decreases. Note that the trend is consistent with the change in crystallinity due to composition change as well as with change in spinning speed. The filaments with higher MPDiol content require higher spinning speeds to achieve a given reduction in shrinkage, and for the higher MPDiol contents, the ultimate shrinkage is not reduced to very low values, even at the highest spinning speeds investigated, due to the lower ultimate crystallinity developed in these resins. The shrinkage of the PET homopolymer drops off to a value of about 3% at the highest take-up velocities. The 4 and 7 mole% MPDiol resins also exhibit low shrinkage at high take-up velocities. Note that the 10 mole% MPDiol filaments never reach as low a value in **Figure 4.10**, presumably due to the development of lower ultimate crystallinity as shown by the X-ray patterns of **Figure 4.9**.

Figure 4.11 shows shrinkage data for filaments spun with a mass throughput of about 6.5 g/min/hole. In general, higher spinning speeds are required to achieve the

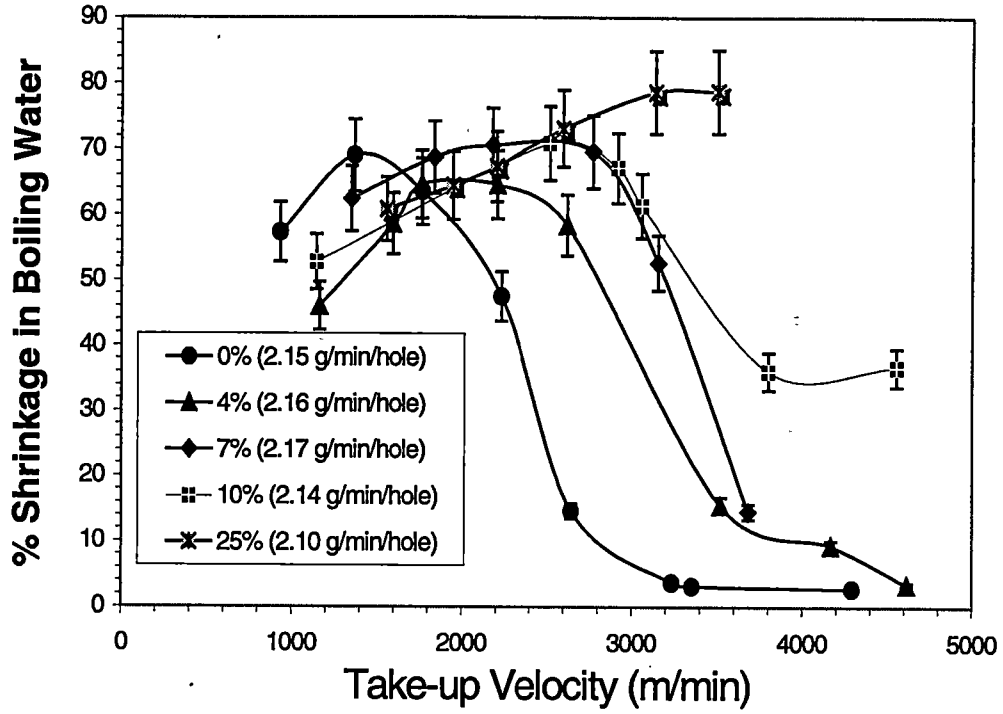


Figure 4.10 Boiling water shrinkage of filaments spun at 2.15 g/min/hole as a function of take-up velocity and MPDiol content.

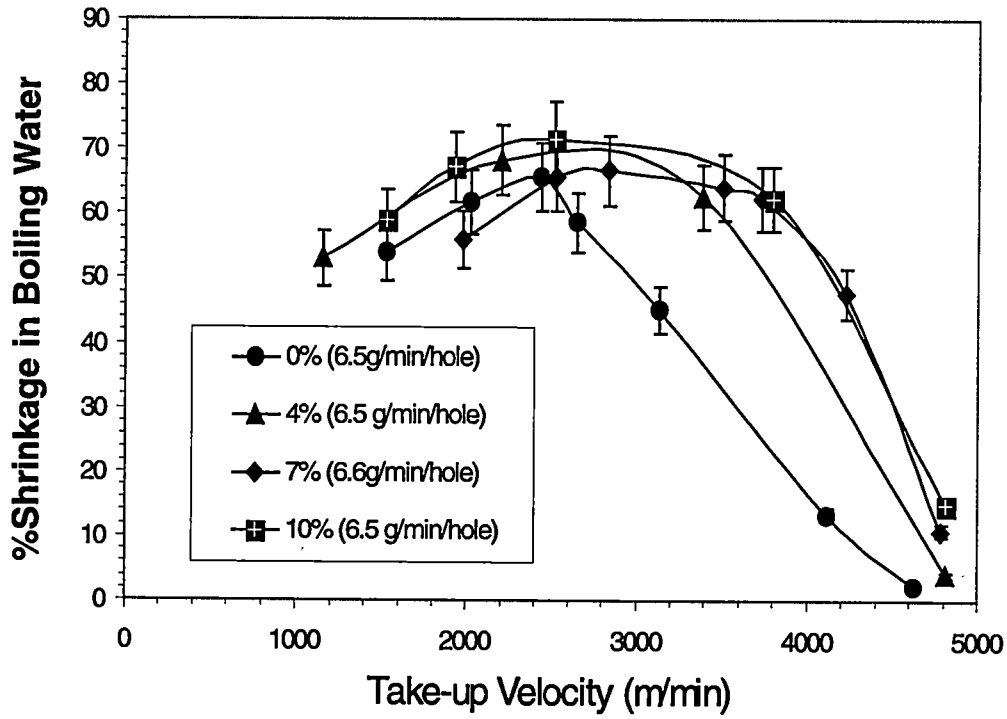


Figure 4.11 Boiling water shrinkage of filaments spun at 6.5 g/min/hole as a function of take-up velocity and MPDiol content.

reduction in shrinkage since the crystallinity develops more slowly at this higher mass throughput due to lower spinline stress at any given spinning speed.

4.2.5 Tensile Properties

The tensile properties of filaments prepared from the PET homopolymer and its MPDiol substituted copolymers are shown in **Figures 4.12, 4.13, 4.14 and 4.15**. The tenacity values increase, while the values of strain at break decrease with take-up velocity. Since the tenacity is determined by (a) the degree of chain extension and (b) the degree of molecular orientation relative to the fiber axis, the results of tenacity measurements correspond closely to expectation based on the birefringence measurements. As would be expected from examination of the birefringence data, the tenacity decreases slightly with increase of MPDiol content, at the same take-up velocity. The strain at break, **Figures 4.14** and **4.15**, does not appear to depend significantly on the MPDiol content.

4.3 Filament Spinnability

All the resins exhibited excellent spinnability. Using the air drag draw-down device and a mass throughput of about 5 g/min/4holes (1.25 g/min/hole) or greater, the filaments could be spun continuously (without fiber breaks) up to the speed corresponding to the maximum air pressure available to our draw down device (80 psig). At a mass throughput of about 3 g/min/4holes (0.75 g/min/hole) filament breaks were observed to occur. The maximum air pressure that could be applied without filament breaks increased as the MPDiol content increased, but, due to the fluctuation of forces on the spinline created by the air drag device, the data were somewhat scattered. For this reason, further studies were carried out using the godet draw-down method.

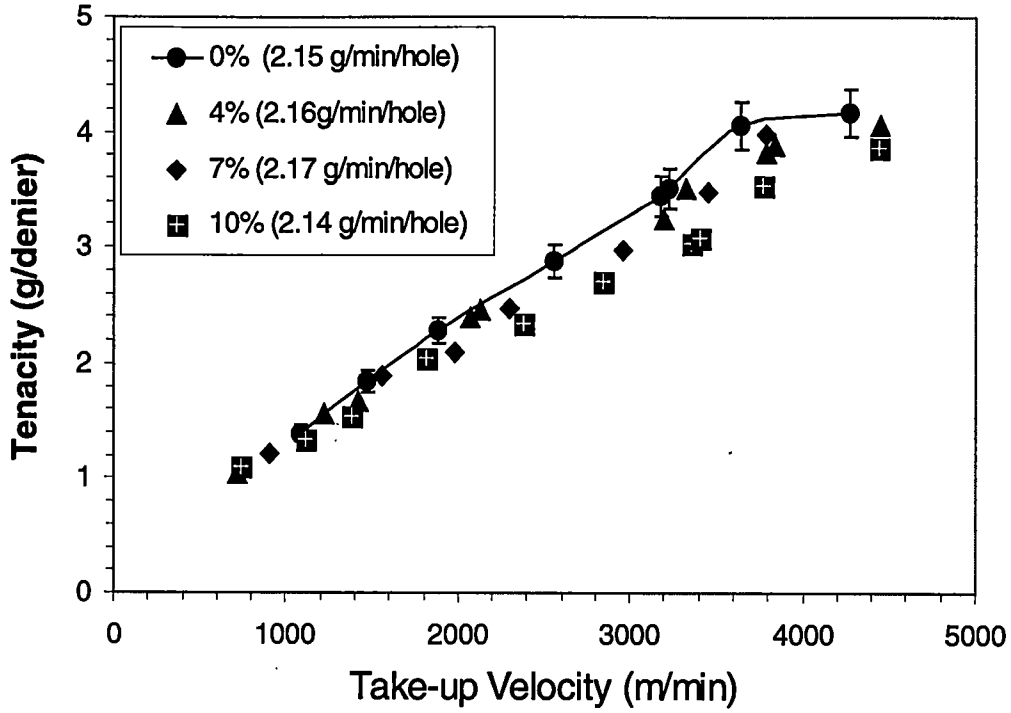


Figure 4.12 Tenacity as a function of take-up velocity and MPDiol content for as-spun filaments prepared with a mass throughput of 2.15 g/min/hole.

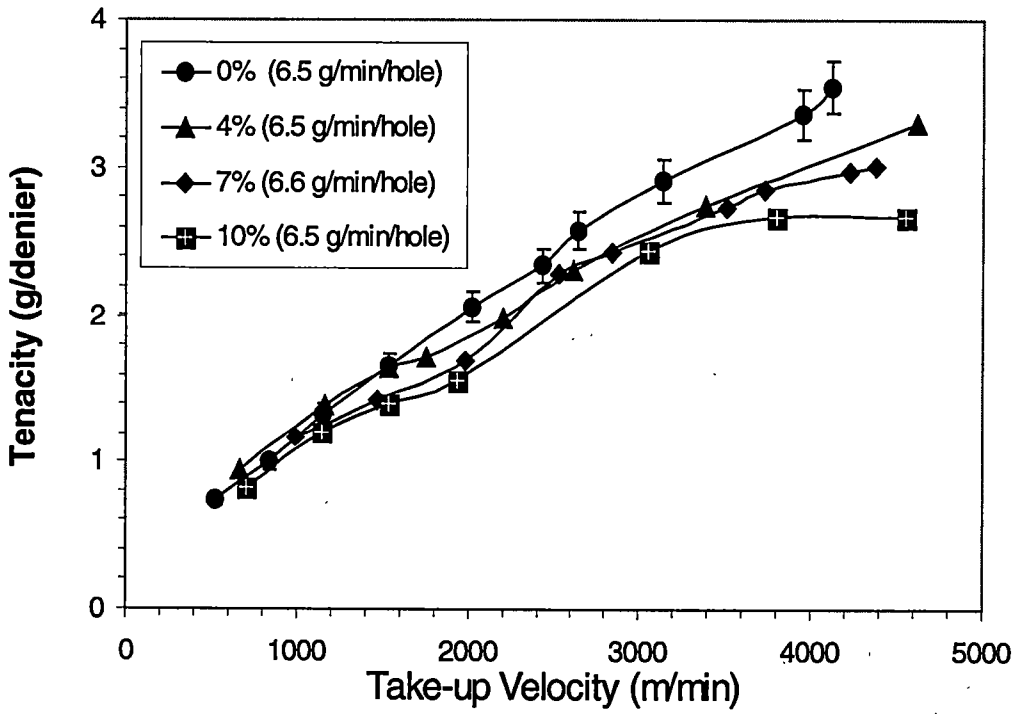


Figure 4.13 Tenacity as a function of take-up velocity and MPDiol content for as-spun filaments prepared with a mass throughput of 6.5 g/min/hole.

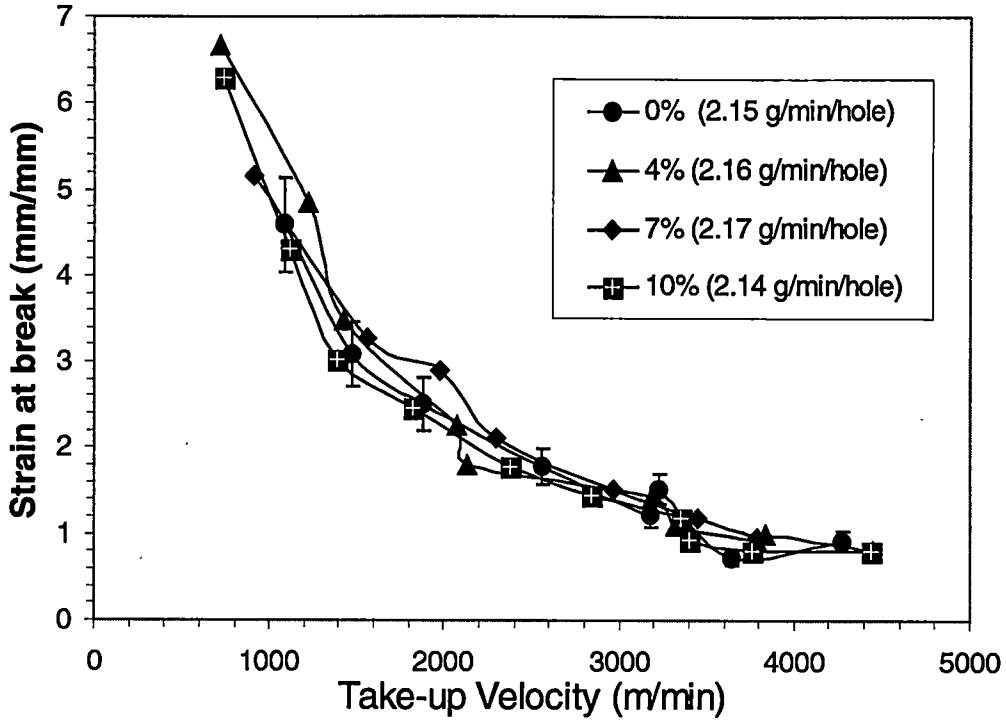


Figure 4.14 Strain at break as a function of take-up velocity and MPDiol content for as-spun filaments prepared with at mass throughput of 2.15 g/min/hole.

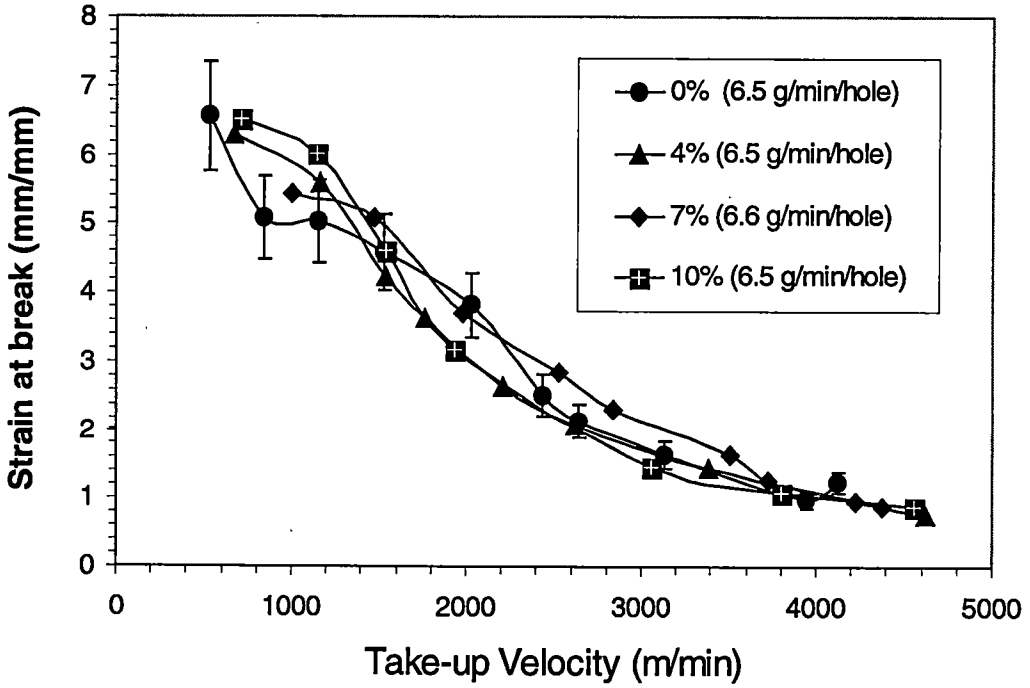


Figure 4.15 Strain at break as a function of take-up velocity and MPDiol content for as-spun filaments prepared with at mass throughput of 6.5 g/min/hole.

Figure 4.16 shows the maximum take-up velocity as a function of MPDiol content at two different mass throughputs for spinning carried out with the godet draw-down technique. The extruder temperature profile and other conditions were kept the same for all runs in order to exclude effects other than the MPDiol content. As shown in **Figure 4.16**, the maximum take-up velocities increase until the MPDiol composition reaches about 7 mol% and then decreases slightly with further increase of MPDiol content. The precise reason for this behavior is not known. However, it may be hypothesized that the slower development of crystallinity allows a greater draw-down and higher take-up velocity before reaching the critical stress for spinline fracture to occur.

4.4 Drawing of Spun Filaments

The PET homopolymer and all MPDiol substituted copolymers except the 25 mol% MPDiol resin were melt spun with mass throughputs of about 8.25 g/min/hole and taken-up at two different take-up velocities to produce eight filament samples for post-spinning drawing experiments. These eight as-spun filament samples are described in **Table 4.1**.

Table 4.1 As-spun filaments wound on bobbins for drawing.

MPDiol Content (mol%)	0	4	7	10
Mass throughput (g/min/hole)	8.25	8.10	8.25	8.10
Lower TUV (m/min)	603	708	591	569
Higher TUV (m/min)	1074	1062	1050	1013

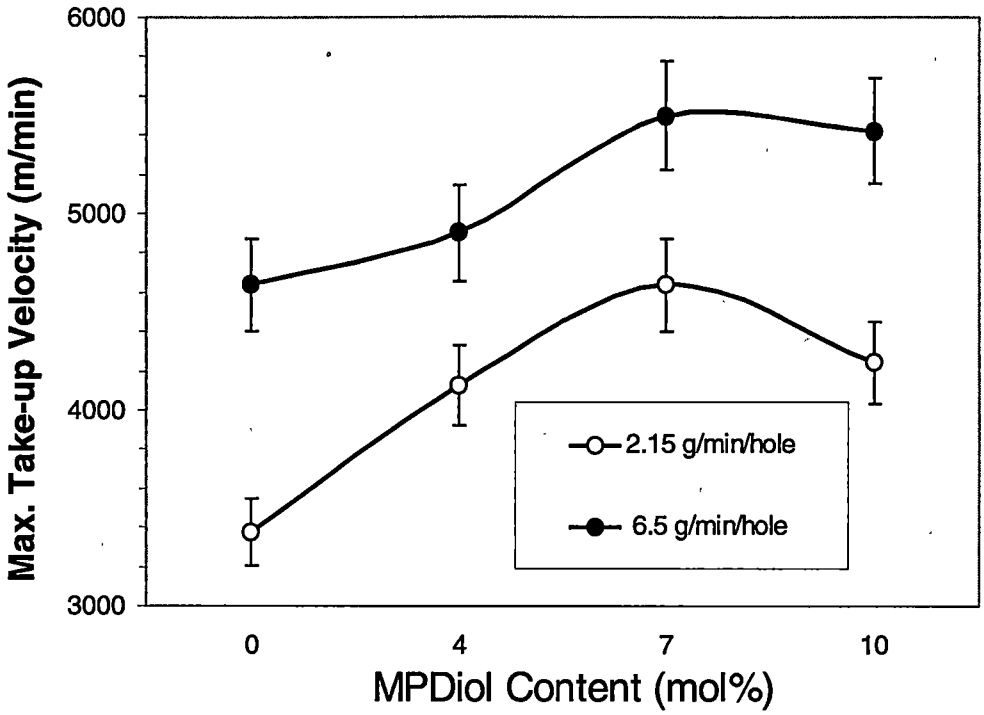


Figure 4.16 Maximum take-up velocity as a function of MPDiol content and mass throughput.

Drawing was carried out using the equipment and methods described in the experimental procedure section. Each of the eight as-spun filaments described in **Table 4.1** were drawn with six different combinations of hot plate and first roll temperatures; these combinations were given in the **Table 3.1**. The overall purpose of these experiments was to find the drawing condition(s) for the optimum mechanical properties of the drawn filaments.

The maximum draw ratio achieved at each combination of draw temperatures, as-spun take-up velocity and MPDiol content are shown in **Figure 4.17**. The results show that the maximum draw ratios were greater for the filaments spun at the lower take-up velocity, as expected. Note, however, that the higher take-up velocity is still below the range where significant crystallinity is developed in the spinning process, even for the PET homopolymer. Consequently, the effect is largely due to higher molecular orientation developed in the filaments spun at the higher spinning speed. From the standpoint of maximum achievable draw ratio, there is a fairly wide window of draw temperature combinations that give nearly equivalent maximum draw ratios. Further, the maximum draw ratios are weakly dependent on the MPDiol content, with the 10% MPDiol resin tending to give slightly higher draw ratios, on the average.

The birefringences of the drawn filaments, corresponding to the maximum draw ratios of **Figure 4.17**, are presented in **Figure 4.18**. The final birefringences of all the drawn fibers are significantly greater than the birefringences of any of the as-spun filaments shown in **Figures 4.3, 4.4, 4.7 and 4.8**. Further, it is clear that drawing at the 80, 110°C (hot plate, first godet) combination is not as effective at producing molecular orientation in the final fibers as several of the other combinations. Apparently, the low

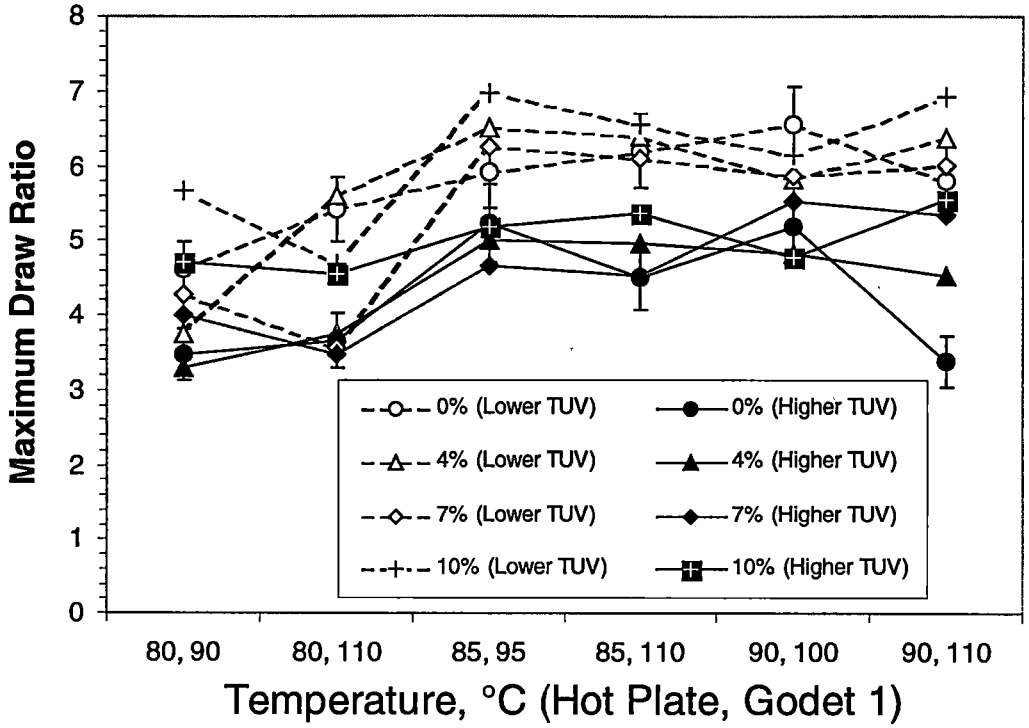


Figure 4.17 Maximum draw ratios as a function of MPDiol composition and different combinations of hot plate and first godet temperatures.

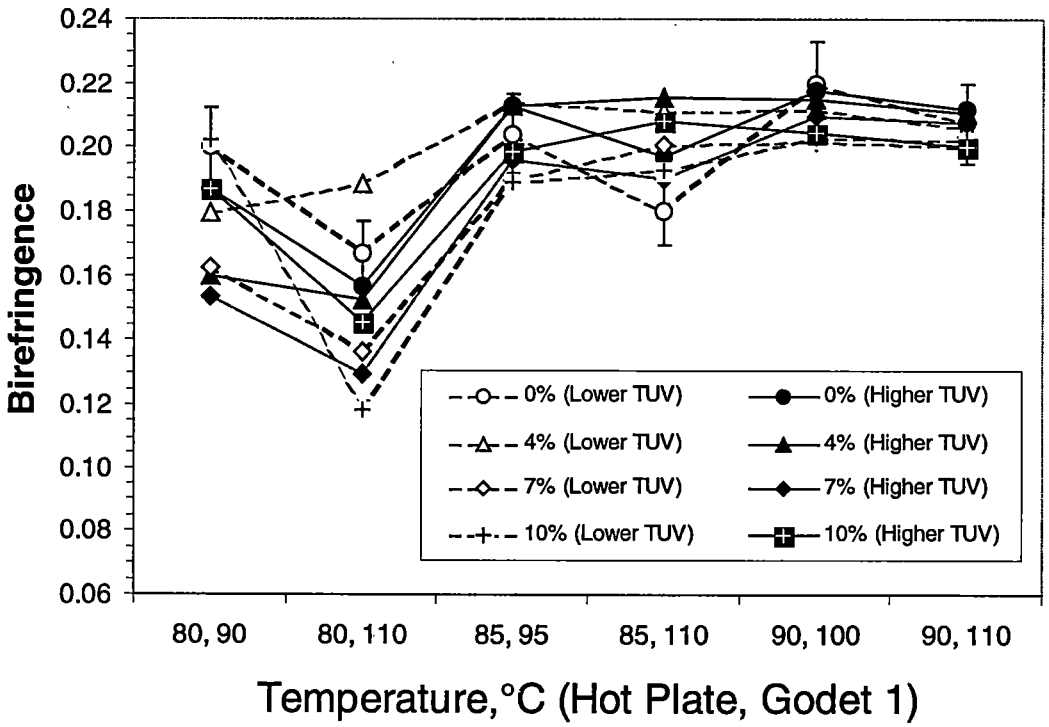


Figure 4.18 Birefringence of fibers drawn with different combinations of hot plate and first godet temperatures.

hot plate temperature combined with the high roll 1 temperature allows significant relaxation of the molecular orientation compared to the cases with a higher hot plate temperature. Based on the birefringence data of **Figure 4.18**, the best drawing conditions examined appear to be with a hot plate temperature of about 90°C and a first godet temperature of about 100°C, though one could argue for slightly different temperatures as a function of MPDiol content.

Of all the drawn samples in PET homopolymer and 10 mol% MPDiol PET, PET homopolymer drawn at 90, 100°C (hot plate, first godet) and 10 mol% MPDiol PET at 85, 110°C (hot plate, first godet) with lower mass throughputs show the highest crystallinity as 39 and 34 % from DSC measurements, respectively. These crystallinities are higher than those obtained from as spun filaments melt spun at high take-up velocities around 4500 m/min. This suggests that the crystalline fraction of as spun filaments increased during the drawing process with the thermal fixation.

Shrinkage measurements on drawn PET homopolymer and 10 mol% MPDiol, which showed the highest crystallinity values in DSC measurements, were also made. The shrinkage values of both drawn filaments decreased down to 13 %, which is attributed to the increase of the crystalline fraction of the filaments. These values, however, are a bit higher than those of as spun filament melt spun at high take-up velocity above 4000 m/min.

Figures 4.19 and **4.20** show the tensile properties of the drawn filaments containing 0 and 10 mole% MPDiol. These data correlate fairly well with the birefringence data, in that the highest tenacity is obtained for a hot plate temperature of

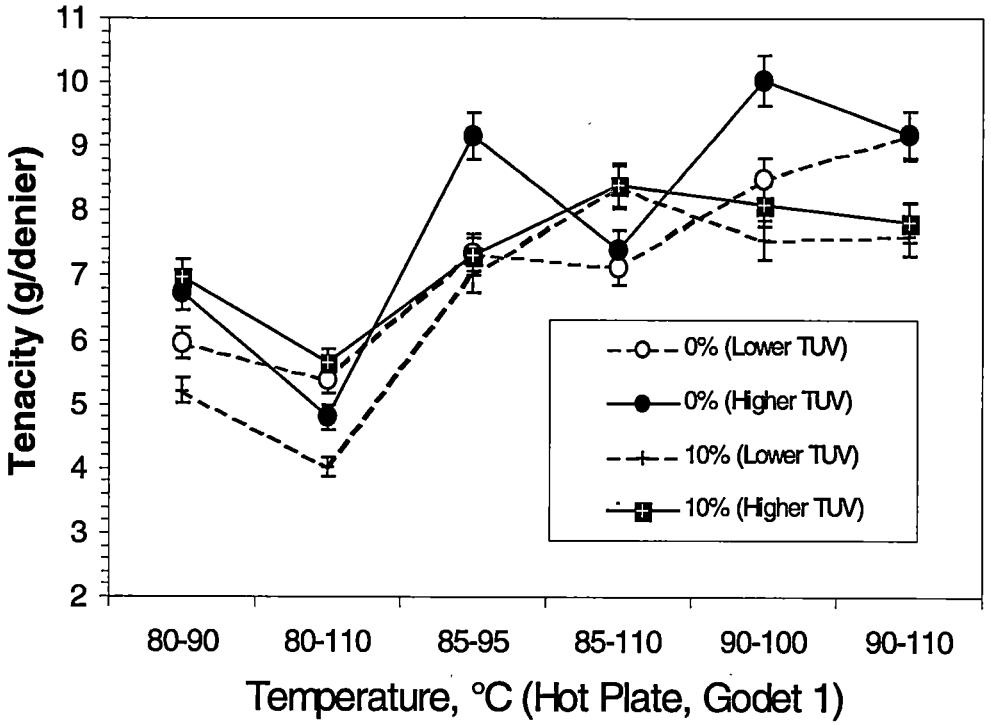


Figure 4.19 Tenacity of drawn filaments of 10% MPDiol compared to filaments of PET homopolymer.

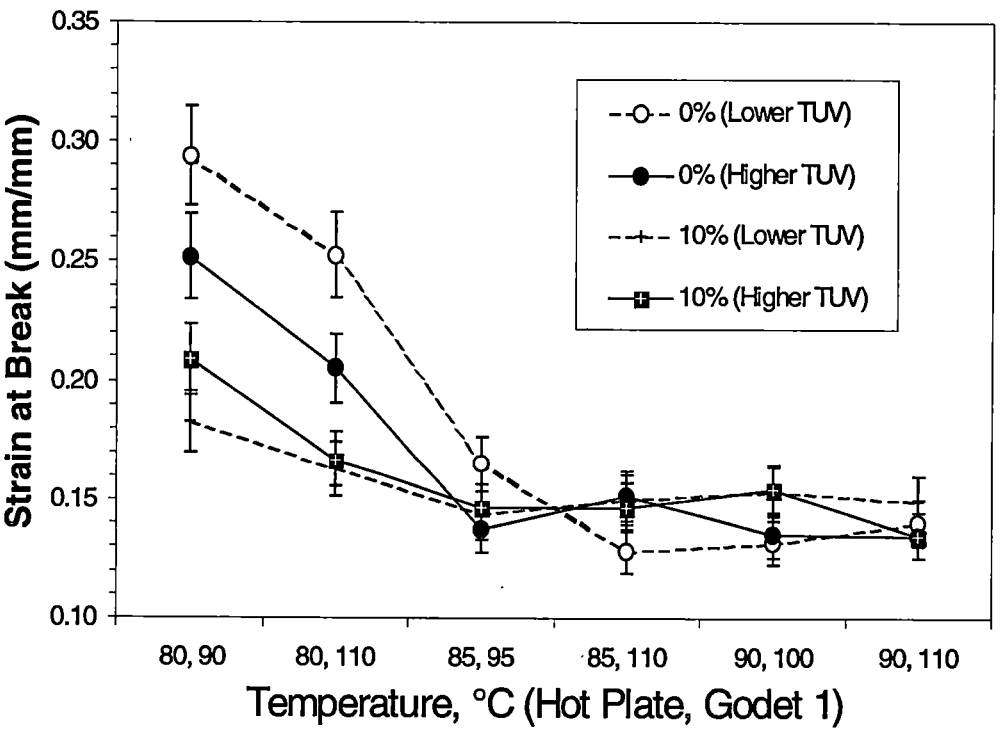


Figure 4.20 Strain at break for drawn filaments of 10% MPDiol compared to PET homopolymer.

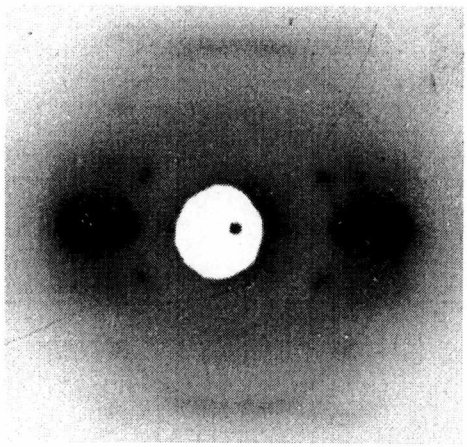
90°C for the PET homopolymer. According to these data, a hot plate temperature of 85°C is better for drawing the 10 mol% MPDiol filaments.

X-ray patterns of selected drawn filaments are shown in **Figure 4.21**. These patterns show that, after drawing, the 10 mol% MPDiol containing filaments have developed almost equivalent crystalline orientation to the PET homopolymer. Further, the crystallinity is also nearly as high.

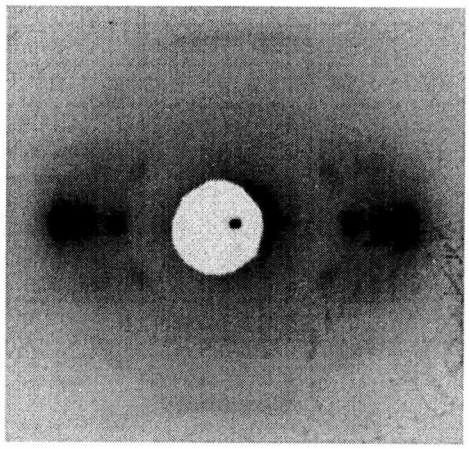
4.5 Further Discussion of Results

One of the ways that the productivity of PET filament yarns can be increased is by increasing the spinning speed [80, 81]. This allows greater throughput with the same size plant and equipment. It is recognized that by reducing the molecular orientation developed during the fiber formation process, higher spinning speeds may be realized. Of course, it is important to maintain the properties of the spun filaments. So the basic idea is to develop a modified PET, which can be spun at higher spinning speeds to achieve the same molecular orientation and properties in the spun filaments, thus improving productivity while maintaining properties. Stated another way, one needs to reduce the level of orientation developed at a given spinning speed, while not changing quantities such as molecular weight that would affect the achievable properties.

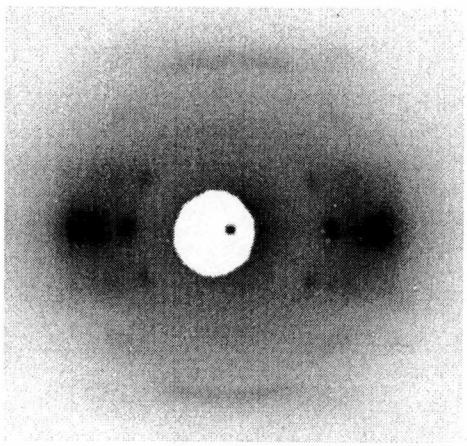
One method to achieve such a reduction in molecular orientation, at a given spinning speed, was described in references 71 and 72, wherein a proprietary material is added to the PET melt via a twin screw extruder. It appears that the substitution of MPDiol for a fraction of the ethylene glycol in PET is another method to achieve this result as is demonstrated in **Figures 4.12, 4.13, 4.14, 4.15** and **4.16**.



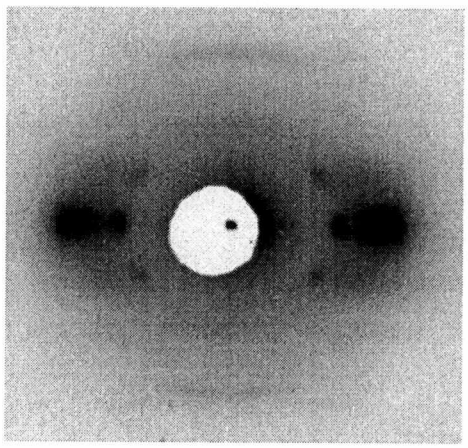
0 mol% MPDiol
90 °C, 100 °C



0 mol% MPDiol
80 °C, 110 °C



10 mol% MPDiol
85 °C, 110 °C



10 mol% MPDiol
90 °C, 110 °C

Figure 4.21 X-ray patterns of selected drawn fibers. The MPDiol content and the combination of hot plate and first godet temperatures are indicated. All filaments were spun with the higher take-up velocity (≈ 1000 m/min).

Another advantage of the ability to spin at higher spinning speeds with the same mass throughput (**Figure 4.16**) is that this allows spinning of finer denier filaments. This produces better comfort in the textile end-use.

For draw-textured yarns, the dyeability of the MPDiol substituted yarns may be better due to the lower crystallinity in the processed filaments. In fact, a recent patent (EP 0 984 086 A1) claims that the substitution of a few mol% MPDiol for ethylene glycol will result in substantial improvement in the dyeability of spun and drawn yarns [71]. The inventors found that 3~5 mol% MPDiol resulted in a 20-27% improvement in dye uptake. This patent also claimed improvement in the tenacity and reduction in the strain at break. However, the present data do not appear to confirm such a claim.

The available data for the present drawn fibers show that the 10% MPDiol resin can be processed to achieve similar mechanical properties to that of the PET homopolymer in fully drawn yarns. From the point of view of mechanical properties, there is no obvious major advantage for the MPDiol substituted resin in fully drawn yarns over the PET homopolymer. However, there may still be other advantages that have not yet been evaluated, such as improvements in dyeability and processing speed.

CHAPTER 5

CONCLUSIONS AND RECOMMENDATIONS

5.1 Summary and Conclusions

It is concluded that:

(1) Within the range of spinning speeds so far achieved, the 25 mol% MPDiol substituted resin does not crystallize in the spinline to any appreciable extent. As a result, it exhibits high shrinkage at all take-up velocities. This result probably precludes the use of resins with this much MPDiol for most fiber applications.

(2) Resins containing 10 mol% MPDiol or less do exhibit appreciable crystallization in the spinline, though the presence of MPDiol reduces the crystallinity compared to filaments prepared from PET homopolymer.

(3) Up to spinning speeds of about 2500 m/min, all resins exhibited similar birefringence. Above this spinning speed, the rate of increase of birefringence with take-up velocity differed for the different resins, with the PET homopolymer having the highest rate of increase. It was suggested that this is due to a greater amount of oriented nucleation and growth of crystals at high spinning speeds in the PET homopolymer than in the copolymer filaments.

(4) Shrinkage in boiling water first increased, reached a maximum and then decreased to much lower values at high spinning speeds (>3000 m/min). The minimum shrinkage achieved does increase as the content of MPDiol increases. It was suggested that the decrease of shrinkage at high spinning speeds is due to the stabilizing effect of crystallization. Higher crystallinity gives greater stability, i.e., lower shrinkage. Thus, the lower crystallinity of the MPDiol containing filaments results in higher shrinkage values.

(5) At the same take-up velocity, a decrease of the mass throughput increases the birefringence and crystallinity and reduces shrinkage.

(6) At the same take-up velocity, increasing MPDiol content decreases crystallinity, birefringence, shrinkage and tenacity.

(7) Higher maximum spinning speeds could be obtained with the addition of MPDiol. The optimum MPDiol content for this purpose appears to be substitution of MPDiol for about 7 mol% of the ethylene glycol that would be present in the PET homopolymer. However, the determination of the precise MPDiol content that would produce the best combination of spinning speed and properties should be further evaluated using commercial scale equipment.

(8) Filaments containing MPDiol can be drawn to give mechanical properties similar to those of PET homopolymer.

(9) The chemical modification of PET studied here can potentially lead to higher productivity in textile yarn spinning due to increased spinning speeds. It may also have the potential to produce yarns with finer denier per filament.

5.2 Recommendations for Further Study

The present laboratory scale effort will conclude with completion of certain tasks and collection of certain data and that is not presently available, including:

(1) Preparation of sufficient drawn fiber of the PET control and the 10 mol% MPDiol resin to allow a preliminary evaluation of the dyeability of MPDiol substituted yarns.

(2) Annealing of as spun filaments of PET control and the 10 mol% MPDiol resin before drawing to investigate the effect of annealing on the crystallinity, shrinkage and tensile properties.

As noted above, it is recommended that the potential for use of MPDiol as a modifier of PET to produce higher spinning speeds and finer denier filaments be pursued. It is important that this phase of the project be carried out using commercial scale equipment similar to that which would be used by a large fraction of commercial converters of polymer to yarns. The complete evaluation of factors such as dyeability that depend on preparation of large quantities of yarn will also require spinning with commercial scale equipment.

LIST OF REFERENCES

1. K. W. Hillier, *Man-Made Fibers*, Vol. 3, Wiley-Interscience, New York, 2 (1967).
2. V. K. Gupta, *Man Made Text*, 554 (1983).
3. E. Izad, *J. Polym. Sci.*, **8**, 503 (1952).
4. W. H. Charch and W. W. Moseley, *Textile Res. J.*, **29**, 536 (1959).
5. D. Coleman, *J. Polym. Sci.*, **14**, 15 (1954).
6. W. Marrs, R. H. Peters and R. H. Still, *J. Appl. Polym. Sci.*, **23**, 1095 (1979).
7. R. E. Wilfong, *J. Polym. Sci.*, **54**, 385 (1961).
8. G. W. Davis and E. S. Hill in M. Grayson, ed., *Kirk-Othmer Encyclopedia of Chemical Technology,* 3rd ed., Vol. 18, Wiley-Interscience, New York, 531 (1982).
9. W. H. Carothers and R. Hill, *J. Am. Chem. Soc.,* **54**, 1579 (1932).
10. J. R. Whinfield and J. T. Dickson, *Brit. Pat.* 578,079 (1946).
11. J. R. Whinfield and J. T. Dickson, *U.S. Patent.* 2,465,319 (1949).
12. C. S. Fuller, *Ind. Eng. Chem.*, **30**, 472 (1938).
13. P. J. Flory, *J. Chem. Phys.*, **15**, 684 (1947).
14. *Brit. Pat.* 682,866.
15. G. G. Odian, *Principles of Polymerization,* 3rd ed., Wiley-Interscience, New York, 97-98 (1991).
16. R. P. Daubeny, C. W. Bunn, and C. J. Brown, *Proc. Roy. Soc.*, Ser. A, **226**, 531 (1954).
17. E. W. Fischer and S. Fakirov, *J. Mater. Sci.*, **11**, 1041 (1976).
18. O. Ishizuka and K. Koyama, *Sen-I Gakkaishi*, **35**, 453 (1979).

19. M. Avrami, *J. Chem. Phys.*, **7**, 1103 (1939).

20. B. Wunderlich, *Macromolecular Physics*, Vol. 2, Academic press, New York (1976).

21. K. Nakamura, K. Katayama and T. Amano, *J. Appl. Polym. Sci.*, **17**, 1031 (1973).

22. G. S. Y. Yeh and K. Z. Hong, *Polym. Engr. Sci.*, **19**, 395 (1979).

23. R. L. Miller, *Flow-Induced Crystallization in Polymer Systems*, Gordon and Breach, New York (1977).

24. G. C. Alfonso, M. P. Verdona and A. Wasiak, *Polymer*, **19**, 711 (1968).

25. K. Nakamura, T. Watanabe, K. Katayama and T. Amano, *J. Appl. Polym. Sci.*, **16**, 1077 (1972).

26. A. Ziabicki, *Fundamentals of Fibre Formation*, Wiley-Interscience, New York, 122 (1976).

27. K. Katayama and M. Yoon, *High-Speed Fiber Spinning – Science and Engineering Aspects*, A. Ziabicki and H. Kawai, Wiley-Interscience, New York, 210 (1985).

28. A. Ziabicki and K. Kedzierska, *J. Appl. Polym. Sci.*, **11**, 14 (1959).

29. S. Kase, *High-Speed Fiber Spinning – Science and Engineering Aspects*, A. Ziabicki and H. Kawai, Wiley-Interscience, New York, 173 (1985).

30. H. H. George, *Polym. Engr. Sci.*, **22**, 292 (1982).

31. J. Shimizu, N. Okui and T. Kikutani, *High-Speed Fiber Spinning – Science and Engineering Aspects*, A. Ziabicki and H. Kawai, Wiley-Interscience, New York, 67 (1985).

32. K. F. Zeminski and J. E. Spruiell, *J. Appl. Polym. Sci.*, **35**, 2223 (1985).

33. R. M. Patel, J. H. Bheda and J. E. Spruiell, *J. Appl. Polym. Sci.*, **42**, 1671 (1991).

34. M. L. Williams, R. F. Landell and J. D. Ferry, *J. Am. Chem. Soc.*, **77**, 3701 (1955).

35. A. Ajji, J. Guevremont, K. C. Cole and M. M. Dumoulin, *Polymer*, **37**, 3707 (1996).

36. H. Janeschitz-Kriegl, *Polymer Melt Rheology and Flow Birefringence*, Springer-Verlag, New York (1983).

37. R. S. Stein and F. H. Norris, *J. Polym. Sci.*, **21**, 381 (1956).

38. T. Kawasaki, *High-Speed Fiber Spinning – Science and Engineering Aspects*, A. Ziabicki and H. Kawai, Wiley-Interscience, New York, 4 (1985).

39. J. E. Spruiell and J. L. White, *Appl. Polym. Symp.*, **27**, 121 (1975).

40. A. Ziabicki and K. Kedzierska, *J. Appl. Polym. Sci.*, **6**, 111 (1962).

41. A. Ziabicki, *Sen-I Gakkaishi*, **38**, 417 (1982).

42. H. M. Heuval and R. Huisman, *J. Appl. Polym. Sci.*, **22**, 2229 (1978).

43. J. Shimizu, N. Okui, T. Kikutani and K. Toriumi, *Sen-I Gakkaishi*, **34**, 64 (1978).

44. K. Nakamura, T. Watanabe, K. Katayama and T. Amano, *J. Appl. Polym. Sci.*, **28**, 2131 (1978).

45. H. H. Hebler, U.S. Patent, 2,604,689 (1952).

46. H. Ludewig, *Polyester Fibers – Chemistry and Technology*, Wiley-Interscience, New York (1971).

47. J. Shimizu, N. Okui, T. Kikutani and K. Toriumi, *Sen-I Gakkaishi*, **33**, 201 (1977).

48. H. H. George, A. Holt, and A. Buckley, *Polym. Engr. Sci.*, **23**, 95 (1983).

49. J. Shimizu, N. Okui, A. Kaneko and K. Toriumi, *Sen-I Gakkaishi*, **34**, 93 (1978).

50. J. Shimizu, N. Okui, A. Kaneko and K. Toriumi, *Sen-I Gakkaishi*, **34**, 64 (1978).

51. J. Shimizu, N. Okui, T. Kikutani, A. Ono and A. Takaku, *Sen-I Gakkaishi*, **37**, 29 (1981).

52. J. Shimizu, N. Okui and K. Tamai, *Sen-I Gakkaishi*, **39**, 398 (1983).

53. J. Shimizu and N. Okui, *Sen-I Gakkaishi*, **39**, 445 (1983).

54. G. Perez and C. Lecluse, *18th Int. Man-Made Fibre Conf.*, Dornbin, Austria (1979).

55. J. Shimizu, *Sen-I Gakkaishi*, **38**, 499 (1982).

56. S. Kase, *High-Speed Fiber Spinning – Science and Engineering Aspects*, A. Ziabicki and H. Kawai, Wiley-Interscience, New York, 67 (1985).

57. A. Ziabicki and J. Tian, *J. Non-Newtonian Fluid. Mech.*, **47**, 57 (1993).

58. S. Zahorski, *J. Non-Newtonian Fluid. Mech.*, **36**, 71 (1990).

59. S. Zahorski, *J. Non-Newtonian Fluid. Mech.*, **50**, 65 (1993).

60. S. Zahorski, *J. Non-Newtonian Fluid. Mech.*, **63**, 33 (1996).

61. D. S. Varma, R. Agarwal and I. K. Varma, *Textile Res. J.*, **56**, 438 (1986).

62. M. Saca and E. Pulat, *J. Appl. Polym. Sci.*, **38**, 539 (1989).

63. G. Hsiue and T. Yeh, *J. Appl. Polym. Sci.*, **37**, 2803 (1989).

64. F. V. Datye and B. H. Palan, *J. Appl. Polym. Sci.*, **38**, 1447 (1989).

65. T. Kiyotsukuri, T. Masuda, and N. Tsutsumi., *Polymer.*, **36**, 262 (1995).

66. M. Gordon and J. S. Taylor, *J. Appl. Chem.*, **2**, 493 (1952).

67. L. Mandelkern, G. M. Martin, and F. A. Quinn, *J. Res.*, **58**, 137 (1957).

68. L. A. Wood, *J. Polym. Sci.*, **28**, 319 (1958).

69. J. H. Gibbs and E. A. Dimarzio, *J. Polym. Sci.*, **40**, 121 (1959).

70. B. Gordon and A. E. Mera, *Polym. Bull.*, **22**, 379 (1989).

71. S. Chen, F. Lin, J. Chou, and H. Wang, *Eur. Pat.* EP 0 984 086 A1 (2000).

72. F-M. Lu and J. E. Spruiell, *J. Appl. Polym. Sci.*, **34,** 1521 (1987).

73. F-M. Lu and J. E. Spruiell, *J. Appl. Polym. Sci.*, **34,** 1541 (1987).

74. S. Misra, F-M. Lu, J. E. Spruiell, G.C. Richeson, *J Appl. Polym. Sci.*, **56,** 1761 (1995).

75. J. E. Spruiell, F-M. Lu, Z. Ding and G. C. Richeson, *J Appl. Polym. Sci.*, **62,** 1965 (1996).

76. F-M. Lu and J. E. Spruiell, *J. Appl. Polym. Sci.*, **49,** 623 (1993).

77. J. H. Bheda and J. E. Spruiell, *J. Appl. Polym. Sci.*, **39**, 447-463 (1990).

78. K. Mezghani and J. E. Spruiell, *J. Polym. Sci. B: Polym. Phys.*, **36**, 1005~1012 (1998).

79. J. Brandrup, E. H. Immergut and E. A. Grulke, *Polymer Handbook*, Wiley-Interscience, New York (1999).

80. W. Stibal, Paper presented in session VIII at the "POLYESTER '98 World Congress", Zurich, Switzerland, December 2-4 (1998).

81. T. Gries, Paper presented in session X at the "POLYESTER '98 World Congress", Zurich, Switzerland, December 2-4, (1998).

VITA

Jaein Suh was born on September 26, 1972 in Seoul, Korea. He attended Hanyang University in Seoul, Korea and received a Bachelor of Science degree in Textile Engineering in August 1997. He enrolled in the graduate college at the University of Tennessee with a major of Polymer Engineering in the fall of 1999. He received his Master of Science degree in Polymer Engineering in August 2001.